Origin of the lithospheric stress field

Carolina Lithgow-Bertelloni and Jerome H. Guynn[1]
Department of Geological Sciences, University of Michigan, Ann Arbor, Michigan, USA

Received 22 February 2003; revised 27 August 2003; accepted 26 September 2003; published 17 January 2004.

[1] An understanding of the tectonic stress field is geologically important because it is the agent that preserves in the crust a memory of dynamical processes. In an effort to elucidate the origin of the present state of stress of the lithosphere we use a finite element model of the Earth's lithosphere to calculate stresses induced by mantle flow, crustal heterogeneity, and topography and compare these to observations of intraplate stresses as given by the World Stress Map. We explore two models of lithospheric heterogeneity, one based directly on seismic and other observational constraints (Crust 2.0), and another that assumes isostatic compensation. Mantle tractions are computed from two models of mantle density heterogeneity: a model based on the history of subduction of the last 180 Myr, which has proved successful at accurately reproducing the present-day geoid and Cenozoic plate velocities, and a model inferred from seismic tomography. We explore the effects of varying assumptions for the viscosity structure of the mantle, and the effects of lateral variations in viscosity in the form of weak plate boundaries. We find that a combined model that includes both mantle and lithospheric sources of stress yields the best match to the observed stress field ($\sim$60% variance reduction), although there are many regions where agreement between observed and predicted stresses is poor. The stress field produced by mantle tractions alone shows a greater degree of long-wavelength structure than is apparent in the stress observations but agrees very well with observations in some areas where radial mantle tractions are particularly strong such as in southeast Asia and the western Pacific. The stress field produced by lithospheric heterogeneity alone depends strongly on the assumed crustal model: Whereas the isostatically compensated model yields very poor agreement with observations, the model based on Crust 2.0 matches the observations about as well as mantle tractions alone and matches very well in certain areas where the influence of high topography is very important (e.g., Andes, East Africa). A possible interpretation of our results is that the stress field is significantly influenced by lateral variations in the viscosity of the mantle, which leads to variable amounts of decoupling between lithosphere and mantle, allowing the mantle signature to dominate in some areas and the crustal signature to dominate in others. The poor fit between the isostatically compensated crustal model and observations and the large differences between the two crustal models point toward the importance of dynamic topography and remaining uncertainties in crustal structure and rheology. We also consider the possibility that observations of stress from the shallow crust may not reflect the state of stress of the entire plate; stresses in the upper plate may be at least partially decoupled from broader-scale plate driving forces by lateral and vertical variations in lithospheric rheology. *INDEX TERMS:* 8120 Tectonophysics: Dynamics of lithosphere and mantle—general; 8164 Tectonophysics: Stresses—crust and lithosphere; 8166 Tectonophysics: Stresses—deep-seated; 8168 Tectonophysics: Stresses—general; *KEYWORDS:* stresses, lithosphere, geodynamics

Citation: Lithgow-Bertelloni, C., and J. H. Guynn (2004), Origin of the lithospheric stress field, *J. Geophys. Res.*, *109*, B01408, doi:10.1029/2003JB002467.

1. Introduction

[2] Stresses in the lithosphere play a key role in many geological processes. The present state of stress of the plates and its recent evolution is important for geological phenomena as diverse as the distribution of earthquakes, mountain building events, sedimentary basin formation and the distribution of fluid reservoirs. On a global scale, the tectonic stress field and its variations are intimately related to the driving mechanism of plate tectonics.

[3] An understanding of the tectonic stress field is geologically important because it is the primary agent of crustal deformation, our primary record of Earth history. The ability

[1]Now at Department of Geological Sciences, University of Arizona, Tucson, Arizona, USA.

0148-0227/04/2003JB002467$09.00

to model the manifestations of intraplate stresses: mountain building, rifting, etc., depends on our knowledge of dynamical processes in the Earth's interior and the surface over geologically long periods of time. The relevant sources of stress span a range of length scales, from global-scale mantle flow to variations in crustal thickness and topography. Mantle sources can be constrained as a function of time as we can compare their effects to other geological and geophysical observables, such as plate velocities, subduction histories, and continental flooding events. On a much shorter length scale, we may find sedimentary basins and complex fault systems, which are associated with rapid spatial variations in stress regimes. A full understanding of all scales of the lithospheric stress field requires input from a variety of sources, including detailed studies of the geologic and structural history of particular provinces, as well as physical modeling of fault initiation and lithospheric processes.

[4] In this study, we focus on sources of stress at wavelengths greater than 200 km, including those associated with mantle flow and lithospheric heterogeneity. The goal of this research is to elucidate the origin and relative contributions to the lithospheric stress field from sources internal to the lithosphere and those from mantle flow. Mantle tractions are derived from mantle flow models that have been previously shown to successfully account for the Earth's geoid anomalies [*Ricard et al.*, 1993], present and past plate motions [*Lithgow-Bertelloni and Richards*, 1998] and Cenozoic true polar wander [*Richards et al.*, 1997]. We consider two very different models of lithospheric heterogeneity, both based primarily on geologic and seismic observations of crustal structure (G. Laske et al., Crust 2.0: A new global crustal model at 2 × 2 degrees, 2002, available at http://mahi.ucsd.edu/Gabi/rem.html). The first uses both the density and crustal thickness of the Crust 2.0 model without any consideration of isostasy while the other uses Crust 2.0 to constrain crustal thickness and Pratt isostatic compensation to constrain crustal density. We explore the influence of radial and lateral variations in viscosity, through different models of mantle viscosity structures, and the incorporation of weak zones in the lithosphere. All our results are compared extensively to the world stress map database (WSM).

2. Previous Work

[5] *Solomon et al.* [1975] and subsequent studies by *Richardson et al.* [1976, 1979] were the first to compute the global lithospheric stress field in the context of models of plate driving forces. They used a parameterized form of the relevant dynamics: Following *Forsyth and Uyeda* [1975], they assign a single global value to each of the assumed plate driving forces (symmetric force at ridges, asymmetric force at trenches (slab pull and suction), and continental and oceanic viscous drag coefficients). The stress field was computed using the thin shell equations. Later models focusing on single plates and based on similar premises [e.g., *Richardson and Reding*, 1991; *Coblentz and Richardson*, 1996; *Meijer et al.*, 1997; *Coblentz et al.*, 1998; *Flesch et al.*, 2000; *Govers and Meijer*, 2001] have included topography and lithospheric density loads as well as a more realistic implementation of the ridge push force. Such nonglobal models for determining stresses have the disadvantage of requiring additional, poorly constrained boundary conditions that are not present in global models [*Richardson et al.*, 1976]. On the other hand, global models need to assume rheological properties at plate margins, which are not well known. In this study, sources of stress deriving from plate driving forces arise self-consistently from a model of mantle flow [*Lithgow-Bertelloni and Richards*, 1998].

[6] Topography and variations in crustal thickness and density have long been recognized as a source of lithospheric stress [e.g., *Jeffreys*, 1959; *Artyushkov*, 1973; *Fleitout and Froidevaux*, 1982, 1983; *Fleitout*, 1991; *Wortel et al.*, 1991]. The magnitude of this contribution remains hard to constrain because of our incomplete knowledge of crustal structure. Moreover, the relative importance of crustal and topographic contributions as compared to other sources of stress is not yet resolved [*Richardson and Cox*, 1984; *Bird*, 1988; *Wortel et al.*, 1991; *Bai et al.*, 1992; *Meijer and Wortel*, 1992; *Richardson*, 1992; *Coblentz and Sandiford*, 1994; *Flesch et al.*, 2000; *Steinberger et al.*, 2001].

[7] Global stress patterns have also been calculated by imposing basal shear tractions either from mantle flow models [*Bai et al.*, 1992; *Steinberger et al.*, 2001; *Yoshida et al*, 2001] or as independent flow velocities [*Bird*, 1998]. In those studies the lithosphere was also treated as a thin shell in a membrane state of stress. *Bai et al.* [1992] showed a relatively poor correlation between the predicted stress directions and the observed regional stress field, possibly due to the wide spacing (15°) of their grid. *Steinberger et al.* [2001] examined stress in the lithosphere due to tractions from the mantle flow induced by density heterogeneity inferred from seismic tomography, as well as due to topography, and found good fits to the global stress field. In contrast to these two works we do not use the thin shell approximation but rather solve the full momentum equation for an elastic lithosphere. Our treatment of crustal and topographic contributions is more complete; we use the most recent compilation of global variations in crustal thicknesses and we examine both isostatic and nonisostatic models. Finally, we use a density heterogeneity model derived from the history of subduction that gives excellent fits to present-day plate motions [*Lithgow-Bertelloni and Richards*, 1998] and geoid anomalies [*Ricard et al.*, 1993].

[8] *Bird* [1998] developed a more complex, global finite element model that included faults at plate boundaries and temperature-dependent viscous rheology, and concluded that some amount of basal driving traction was required to achieve a reasonable match to stress observations. However, models with driving shear tractions implemented NUVEL-1 [*DeMets et al.*, 1990] velocities on the plates rather than calculating them from mantle flow. The shear stress was calculated by using only the difference in velocity between the plate and mantle at 400 km depth and imposed artificial NUVEL-1 velocity directions at 400 km for the best fit models. In contrast to this study our mantle flow models are an accurate solution to the Stokes equation given a prescribed density field.

3. Theory

3.1. Governing Equations

[9] Our model is governed by the equations of conservation of mass and momentum

$$-\rho g \hat{e}_r + \frac{\partial \sigma_{ij}}{\partial x_j} = 0 \qquad (1)$$

$$\frac{\partial v_i}{\partial x_i} = 0 \tag{2}$$

where we have assumed incompressibility and that gravity is the only significant body force and we have adopted the Einstein summation convention; σ_{ij} is the stress tensor, g is the acceleration due to gravity, v_i is the velocity field, and ρ is the density, and we have neglected accelerations. The stress tensor

$$\sigma_{ij} = -P\delta_{ij} + \tau_{ij} \tag{3}$$

consists of a hydrostatic part (negative of the pressure) and a deviatoric part, τ_{ij}; the latter being the primary quantity of interest. We solve these equations together with the following constitutive relation for the lithosphere:

$$\varepsilon_{ij} = \frac{1+\nu}{E}\sigma_{ij} - \frac{\nu}{E}\sigma_{kk}\delta_{ij} \tag{4}$$

where we have assumed that the lithosphere is elastic and that the velocity field in this portion of the solution domain is piecewise continuous in space. The elasticity of the lithosphere is assumed to be isotropic, and linear: the strain, ε_{ij}, is related to the stress by Poisson's ratio, ν, and Young's modulus, E; δ_{ij} is the Kronecker delta. In most models we further assume that the elasticity of the lithosphere is homogeneous. We have also examined the effect of weakened plate boundaries in which the Young's modulus is assigned a reduced value.

[10] While the pressure and temperature conditions in most of the lithosphere, or even the lower crust, are conducive to viscous flow, and plastic deformation is observed at plate boundaries, the plates as a whole exhibit elastic behavior, even over geologic timescales. They have little internal deformation [*Gordon*, 1995; *DeMets and Dixon*, 1999], even for intraplate regions with relatively high seismicity such as the New Madrid zone [*Newman et al.*, 1999; *Weber et al.*, 1998]. In addition, the earthquakes used to gain stress information are elastic events that occur over short timescales. Therefore, while a simplification, a purely elastic rheology is a good approximation.

[11] The governing equations are solved via the finite element method, as described in section 3.2, subject to boundary conditions that are free slip at the surface, and no-slip at the base of the lithosphere. Sources of stress in the lithosphere include horizontal and radial basal tractions from mantle flow and buoyancy within the lithosphere including contributions from surface topography, lateral variations in crustal thickness, and intralithospheric variations in density. We have neglected the potential effect of edge tractions such as collisional resistance at convergent boundaries, largely because for our forward model we have no good theoretical basis for inferring the effect of forces at the edges and there are no good empirical constraints. In other words, while a model that incorporated all the details of lithospheric and mantle rheology realistically would contain all relevant tractions, the relevant rheology is not sufficiently known. We note that ridge push, which is sometimes treated as an edge force, is properly included in our models as the effect of lithospheric thickening.

[12] Because many studies have used the thin shell approximation to the governing equations, and because this form imparts considerable physical insight into the expected behavior of the lithosphere, we briefly discuss this approximation here. The Earth's lithosphere is sufficiently thin as compared with its radius of curvature that it should approximate a membrane state of stress in which the lithosphere does not support bending moments. In this case the momentum equation reduces to [*Love*, 1944]

$$N_{\theta\theta} + N_{\phi\phi} = -q_r R \tag{5a}$$

$$\frac{\partial}{\partial\theta}(N_{\theta\theta}\sin\theta) + \frac{\partial N_{\theta\phi}}{\partial\phi} - N_{\phi\phi}\cos\theta = -q_\theta R\sin\theta \tag{5b}$$

$$\frac{\partial}{\partial\theta}(N_{\theta\phi}\sin\theta) + \frac{\partial N_{\phi\phi}}{\partial\phi} + N_{\theta\phi}\cos\theta = -q_\phi R\sin\theta \tag{5c}$$

$$N_{ij} = H\tau_{ij} \tag{5d}$$

where R is Earth's radius, H is the thickness of the lithosphere, θ is the colatitude, ϕ is the longitude, and q is the vector of applied tractions. For the stress resultant, N_{ij}, we have departed from some previous notation by uniformly using two indices since this quantity is properly a tensor and to clarify its relationship to the stress field. Two special cases are relevant to subsequent discussions. If $q_r = 0$, the two horizontal stresses are equal in magnitude and opposite in sign, producing pure strike-slip behavior. If $q_\theta = q_\phi = 0$, the horizontal stresses are equal in magnitude and sign, producing pure compression or pure extension, depending on the sign of q_r.

3.2. Sources of Stress

3.2.1. Horizontal Tractions

[13] The shear tractions at the base of the lithosphere that are generated by mantle flow may be described as containing two contributions (Figure 1):

[14] 1. Driving tractions are generated by viscous flow in the mantle driven by mantle density heterogeneity. The driving tractions may oppose plate motion over a portion of the plate depending on the pattern of mantle density heterogeneities that drive the flow (Figure 1a).

[15] 2. Resisting tractions are generated by the motion of the plates on the viscous mantle, and are opposite to the direction of motion of that plate at each point, and are proportional to the local speed of the plate (Figure 1b). Plate velocities are determined by the balance of driving and resisting torques, i.e., the net tractions (the sum of driving and resisting tractions at each point) over the surface of the plate [e.g., *Ricard and Vigny*, 1989; *Forte et al.*, 1993; *Lithgow-Bertelloni and Richards*, 1998]. It is the net tractions that generate stresses in the lithosphere.

3.2.2. Radial Tractions

[16] Because the lithosphere has negligible flexural strength on long wavelengths, it provides little resistance to radial tractions applied at its base. Radial tractions then result in topography that is dynamically, rather than statically, supported [e.g., *Lithgow-Bertelloni and Silver*, 1998].

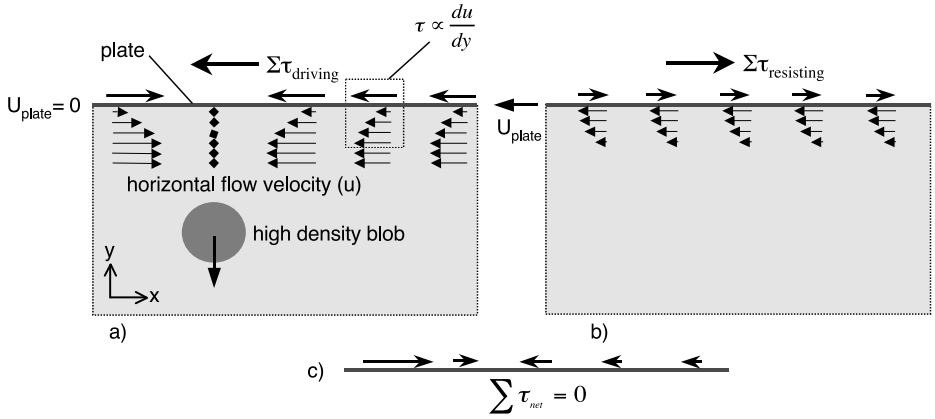

Figure 1. Horizontal tractions and their relationship to mantle flow and plate motion. The tractions can be thought of as being composed of two contributions: (a) driving tractions due to mantle density heterogeneity and resultant flow and (b) resisting tractions that oppose plate motion. While resisting tractions oppose plate motion at every point, the converse is not true of the driving tractions, they may locally oppose plate motion. (c) Net tractions, which are the sum of driving and resisting tractions and must integrate to zero over the area of the plate if the plate is to move at constant velocity. In the example shown, a dense anomaly located under the western portion of a plate drives the plate westward, although they locally oppose plate motion to the west of the anomaly. Resisting tractions are homogeneous in this two-dimensional example, although they would vary in proportion to the local velocity in a three-dimensional plate as it rotates about its Euler pole.

The magnitude of this topography h_d is a balance between the radial traction driving the deflection and gravity as a restoring force

$$h_d = \frac{-q_r}{\Delta\rho g} \tag{6}$$

where $\Delta\rho$ is the density contrast between the lithosphere and the surface (atmosphere or ocean). The displacement of the lithosphere results in two types of horizontal stresses within the lithosphere, as shown in Figure 2. The first are gravitationally induced stresses due to topography, the same gravitational sliding mechanism that leads to the "ridge-push" force in oceanic lithosphere. The second are membrane stresses due to the lithosphere being extended or compressed.

3.2.3. Topography and Intralithospheric Heterogeneity

[17] Lateral variations in density and topography produce lateral variations in the outward traction exerted on neighboring columns that must be balanced by horizontal deviatoric stresses (Figure 3). Assuming a lithostatic reference state, in two dimensions we have,

$$\sigma_{xx} = \sigma_{zz} + \tau_{xx} \tag{7}$$

where σ_{zz} at any depth is due to the overburden. A static force balance yields [*Turcotte and Schubert*, 1982]

$$\frac{dN_{xx}}{dx} = \frac{d\Omega}{dx} \tag{8}$$

where

$$\Omega = -\int_{-D}^{h} dz \int_{z}^{h} g\rho(z')dz' \tag{9}$$

is the gravitational potential energy per unit area (GPE) [*Molnar and Lyon-Caen*, 1988]. Below, we consider the quantity Ω/H, the mean outward traction exerted by the lithospheric column, where $H = D + h$ is the thickness of the lithosphere. N_{xx} is the stress resultant

$$N_{xx} = \int_{-D}^{h} \tau_{xx} dz \tag{10}$$

h is the height of topography, and D is the depth of compensation below which significant deviatoric stress is

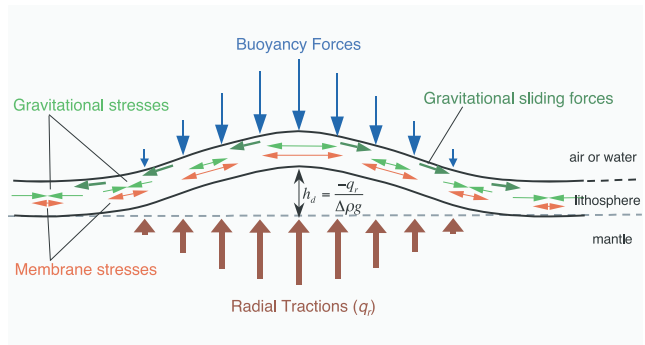

Figure 2. Forces, tractions, and resulting stresses associated with dynamic topography. Radial tractions are opposed by buoyancy; the balance between these two forces yields a dynamic topography h_d. The topography, which is greatly exaggerated, produces two types of stresses: membrane stresses due to stretching of the lithosphere and gravitational stresses due to the topographic gradient. Stresses in the lithosphere are constant throughout the thickness (no bending stresses).

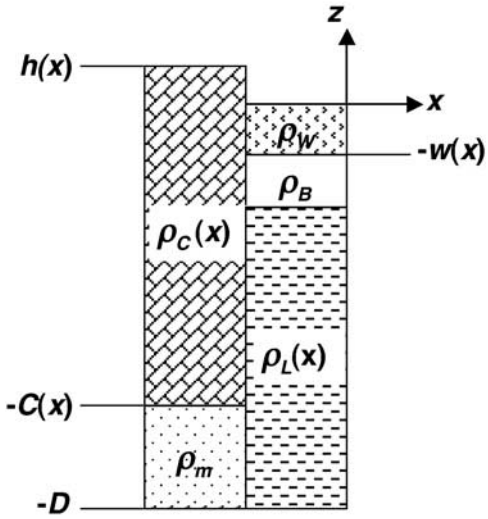

Figure 3. Schematic representation of lithospheric and mantle structure for (left) a continental and (right) an oceanic column. The density of seawater, $\rho_w = 1020$ kg m^{-3}, oceanic crust, $\rho_b = 2880$ kg m^{-3}, and subcontinental mantle, $\rho_m = 3300$ kg m^{-3} are assumed constant, whereas the density of the continental crust, ρ_c, and of the oceanic lithosphere, ρ_L, may vary laterally. We assume that $\rho_L = \rho_m$ at the ridge and that ρ_L increases with increasing age of the lithosphere according to a half-space cooling model. Topography h and the depth to the base of the continental crust $-C$ vary laterally, and we assume that the depth of compensation $D = 100$ km is constant.

not supported (compensation depth), and we have assumed that D does not vary laterally. The two-dimensional equations illustrated above are helpful in introducing the GPE, Ω. In our calculations the GPE is implemented in the finite element model, which solves equations (7)–(8) with the appropriate generalizations for three dimensions in a spherical shell.

[18] Although none of our results are based on it, we may nevertheless derive some insight from the special case of an isostatically compensated homogeneous crust, which permits an analytical solution [*Artyushkov*, 1973]. Thickening of the crust and increases in surface elevation make the deviatoric stress more tensional, while thinning and lowering of surface topography make the stress more compressional.

4. Computational Methods

4.1. Mantle

[19] The horizontal and radial tractions arising from mantle flow and that we apply at the base of the lithosphere were computed as in [*Lithgow-Bertelloni and Richards*, 1998]. Given a prescribed density heterogeneity field the induced viscous flow can be solved analytically via propagator matrices [*Hager and O'Connell*, 1979, 1981]. The net shear and radial tractions due to the instantaneous mantle flow in the presence of plates are computed to spherical harmonic degree and order 20, corresponding to wavelengths of ~2000 km [*Lithgow-Bertelloni and Richards*, 1998]. The net tractions include both the effects of density heterogeneity and plate motions. The plate motions we use are those consistent with the flow model generated by the density heterogeneity, in other words, the velocities required for exactly balancing driving and resisting torques [*Lithgow-Bertelloni and Richards*, 1998]. We do not impose observed plate motions. We have not included the effects of self-gravitation, which are less than 20% for radial tractions. Self-gravitation is primarily important at low harmonic degrees.

[20] An unavoidable consequence of any model that combines a piecewise surface velocity field with a Newtonian fluid is a divergence of the driving tractions at plate boundaries. This phenomenon was studied by *Hager and O'Connell* [1981], who showed that the stress diverged logarithmically with the maximum harmonic degree of the fluid velocity field. In our work, we have chosen a maximum harmonic degree ($l = 20$) that produces stresses at plate boundaries that are not unphysically large and that lead to the best fit to the plate velocities [*Lithgow-Bertelloni and Richards*, 1998]. The choice of a maximum harmonic degree is not unlike specifying a yield strength for mantle material that limits the magnitude of stresses that can be supported. Another possible approach would be to modify the assumed rheology in such a way that a yield strength is explicitly included. In any case, our investigation of the effects of weak plate boundaries suggests that the lithospheric stress field does not depend strongly on the details of our approach.

4.2. Lithosphere

[21] We solve for the stresses in the lithosphere on a spherical shell via the finite element method using the commercial finite element program ABAQUS [*Hibbit and Sorenson*, 2002]. In contrast to studies of individual plates [e.g., *Flesch et al.*, 2000; *Coblentz and Sandiford*, 1994; *Richardson and Reding*, 1991; *Govers and Meijer*, 2001], there are no edge boundary conditions.

[22] The FEM of the lithosphere is composed of three-dimensional, 8 node quadratic continuum elements. The top and bottom surfaces of the mesh are quadrilaterals that are nearly equal area, as shown in Figures 4a and 4b for a 2° (~220 km on an edge) surface mesh, similar to that of *Zhong et al.* [2000]. The surface mesh is projected inward to form the three-dimensional element shape; the thickness is a constant 100 km in all models. While the average elastic thickness of the lithosphere may be closer to 50 km, a thinner lithosphere would influence stress magnitudes and orientations at wavelengths shorter than those investigated here [*Zhong and Zuber*, 2000]. An enlarged portion of the mesh is shown in Figure 4c, superimposed on the continents and plate boundaries, along with the elements that were used to investigate plate boundaries as weak zones. The elements were not modified to precisely fit the plate geometry since they were only used to study the first order effects of plate boundaries as weak zones. The elements have a Young's modulus, $E = 1 \times 10^{11}$ Pa and a Poisson's ratio, $\nu = 0.3$, typical values for crustal rocks. For a homogeneous lithospheric rheology, the values of E and ν do not affect the stresses, only the deformations, which are linearly dependent on their values. We also investigated a lithosphere with multiple layers to assess the depth dependence of the stress at long wavelengths. At long wave-

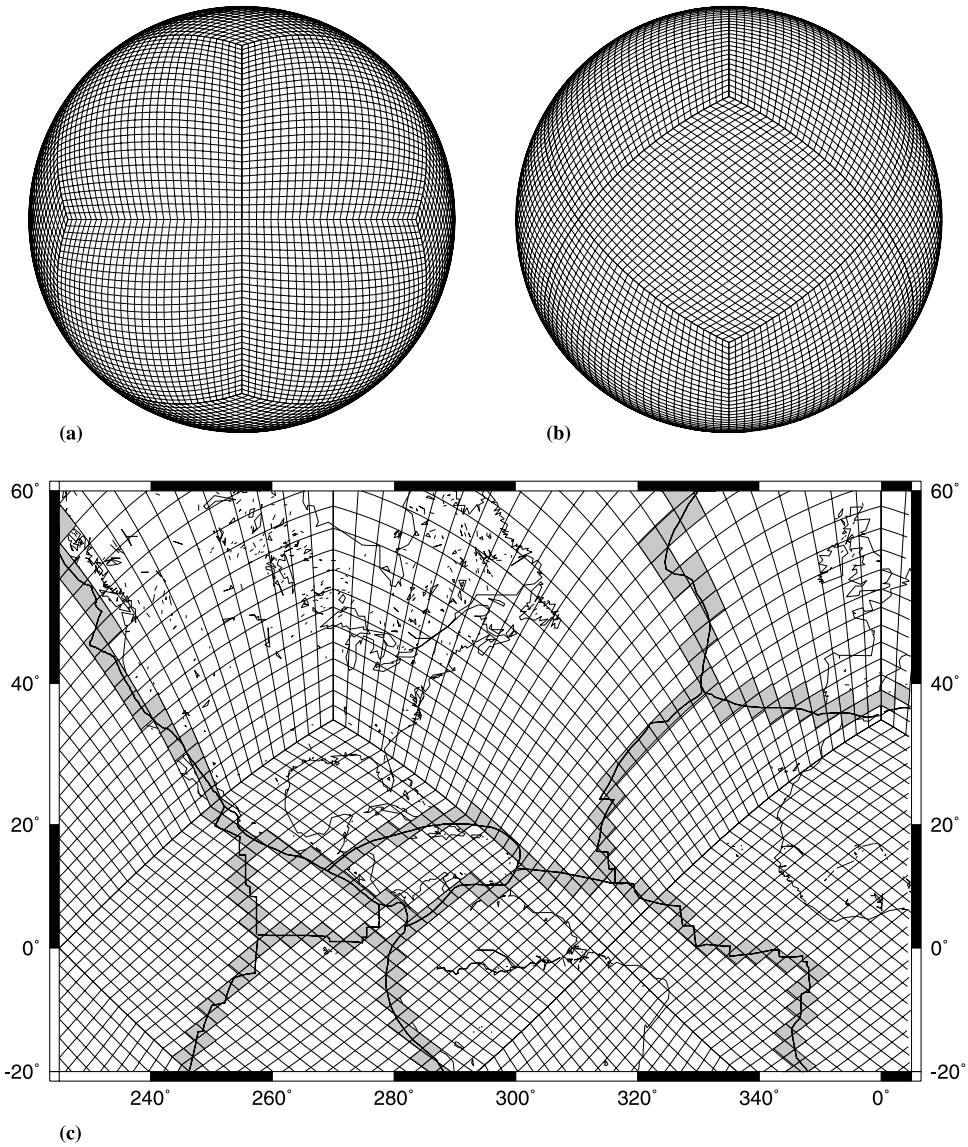

Figure 4. Global finite element mesh with approximately 2° spacing (9408 elements). The sphere is divided into 12 equal-area diamonds using equal length great circle arcs. Each of the diamonds is subdivided into 121 elements, 28 per arc, using the same length great circle arcs. The resulting elements are close to equal-area and have minimal distortion. (a) Polar view; (b) intersection of the equator and the prime meridian; and (c) detail with continents and plate boundaries superimposed showing the location of weak elements in the model that includes lateral variations in lithospheric strength.

lengths, for constant rheology and no discontinuities, stress results should not vary from top to bottom. This was indeed the case for a model with five 20 km lithospheric layers.

[23] The chosen three-dimensional (3-D) elements have the advantage over 2-D elements of providing an exact solution, allowing thickness variations, making it easier to implement lateral stresses due to topography and density variations, as well as allowing for viscoelastic rheology. Although we have not made full use of the three-dimensional capability in this study (for example, representing the lithospheric contribution as a vertical average), the important point is that our approach is general and will allow for the incorporation of structural and rheological complexity in future studies. Since shear tractions cannot be applied to the base of the 3-D elements in ABAQUS, the mantle tractions are modeled as body forces applied to a layer of thin shell elements with negligible thickness (1 km) at the base of the 3-D lithospheric elements (Figure 5). The term thin shell element here is the proper technical term for these elements in ABAQUS; it does not imply that the solution to the momentum equation for the entire domain is based on the thin shell approximation.

[24] In order to constrain the model from free body translation and rotation the mesh must be pinned. Even if all forces and moments are formally balanced, the finite numerical precision and associated round-off errors in the calculation result in translation and rotation. If a single node is pinned, erroneous stress concentrations will occur around that node, even for very small net torques. To resolve this problem, a base layer of 3-D continuum elements with very

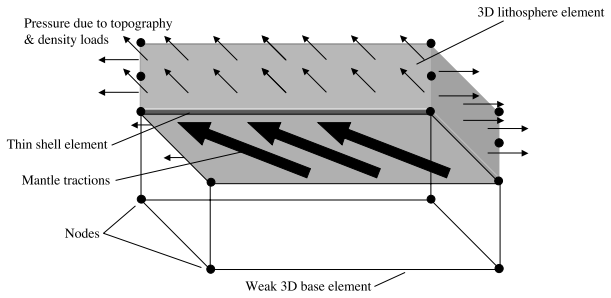

Figure 5. Diagram of the finite element model and applied forces for one lithospheric block, consisting of one lithospheric element (100 km thick), a single thin shell element, and a single base layer.

low Young's modulus (10^5 smaller than lithospheric elements) is applied below the lithospheric layer (Figure 5). The top nodes are connected to the 3-D lithospheric elements and the bottom nodes are pinned. This distributes the residual forces evenly over all elements. The presence of the weak base layer does not affect stress orientations and magnitudes as long as the ratio of Young's modulus between the lithospheric elements and the weak elements exceeds 1000 (Figure 6).

4.3. Applied Loads

4.3.1. Mantle Tractions

[25] We investigated two different density heterogeneity fields, one derived from the history of subduction (SLB) [*Lithgow-Bertelloni and Richards*, 1998], and the other derived from the seismic tomographic model of *Grand et al.* [1997] (TMG) using an assumed scaling of velocity to density anomalies of 0.4 g cm^{-3} s km^{-1} [*Ricard et al.*, 1989] and excluding the top 250 km, where chemistry rather than temperature controls lateral variations in velocity, and strong lateral viscosity variations might be important. The computed tractions also depend on the assumed viscosity structure of the mantle. We investigated two different viscosity structures for the SLB model. The first has a lithosphere 10 times more viscous, and a lower mantle 50 times more viscous than the upper mantle. This viscosity structure yields the best fit to observed geoid anomalies [*Ricard et al.*, 1993] and Cenozoic plate motions (for an absolute upper mantle viscosity of 4.2×10^{20} Pa s) [*Lithgow-Bertelloni and Richards*, 1998] and has been used to explain true polar wander for the past 100 million years [*Richards et al.*, 1997]. The second viscosity structure we investigated is identical except that it includes a low-viscosity channel from 100 to 200 km depth with a viscosity 100 times less than the upper mantle (LVC).

[26] The radial components of the basal tractions require special treatment. Because the computation does not include gravity explicitly as a body force, there is no restoring force opposing radial tractions aside from the weak elastic response. The influence of radial tractions was accounted for by displacing the nodes of the elements by an amount equal to the dynamic topography, computed from equation (6). This deflection results in membrane stresses that may be added to those generated by other loads since the rheology and governing equations are linear. The gravitational stresses associated with dynamic topography are computed in the same manner as those associated with other sources of lithospheric heterogeneity (equation (9)).

[27] The corresponding net shear and radial tractions at the base of the lithosphere for the subducted slab history are shown in Figure 7. Prominent features of the radial tractions are broad upwellings in the Atlantic basin, in the middle of the Pacific plate and under the western and southern part of the African plate and more focused downwellings near current and extinct trenches, particularly the large area around southeastern Asia. Magnitudes are in the range 0–50 MPa, with downwellings being much stronger than upwellings since this model is based on density heterogeneity due to slabs without sources of active upwelling: the upwellings in this model are passive and the result of return flow from slabs. The horizontal net tractions are greatest in the vicinity of current or past subduction and at ridges. The former are due primarily to the driving forces associated with sinking slabs, while the latter are primarily due to resisting forces since the driving forces are small at ridges in the subduction history model. The pattern of horizontal net tractions at ridges is particularly sensitive to the assumed density heterogeneity field. For the tomographic model of density heterogeneity (TMG), low-velocity anomalies lead to broad upwelling and driving tractions at ridges that largely cancel the resisting tractions. While the magnitude of resisting tractions at plate boundaries depends on the value of the maximum harmonic degree in the flow calculations, it is important to recognize that the presence of such

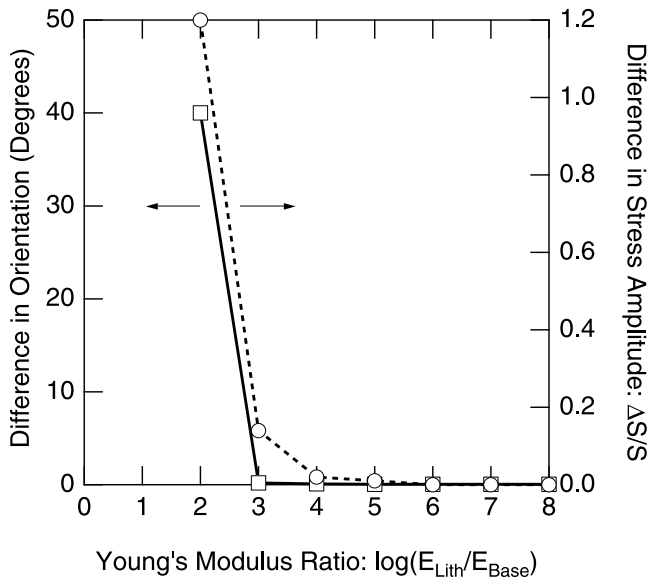

Figure 6. Effect of base element Young's modulus on computed stresses: (right axis, dashed line) ratio of the RMS difference in stress magnitude to the average stress magnitude computed as the root of the second invariant; (left axis, solid line) relative difference in orientation of the principal stress directions. Both quantities are referred to results in the limit E_{Base}–>0. For E_{Lith}/E_{Base} = 1000, the orientation reaches this limit to within numerical precision and the difference in stress magnitudes is small. In all our calculations, we used $E_{Lith}/E_{Base} = 10^5$.

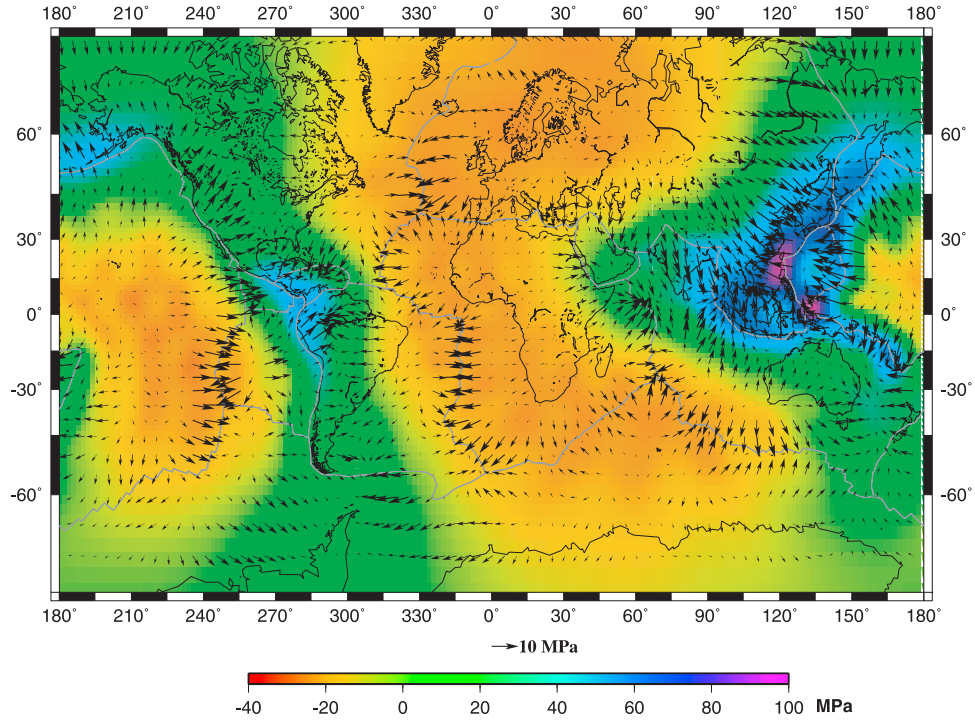

Figure 7. Net tractions for model SLB. Arrows show the direction and magnitude of horizontal tractions; color contours give the value of the radial tractions. Radial tractions are positive downward.

tractions are expected since plate boundaries must be associated with large spatial gradients in the mantle flow field. Moreover, the pattern of net tractions that we find suggest that the magnitude of resisting tractions at plate boundaries is not unreasonable: they are comparable to other tractions in the model and sufficiently similar to driving tractions that they may be canceled depending on assumptions of the density heterogeneity field. The magnitude of resisting tractions at ridges may also be reduced by lateral variations in viscosity near the ridge, such as a lowering of viscosity associated with the presence of partial melt.

4.3.2. Topography and Lithospheric Heterogeneity

[28] Lateral heterogeneity in the lithosphere generates stresses through the action of gravity. However, applying the body force directly to the elements of a finite element model generates numerical instabilities within the mesh related to the compression and relaxation of the material, a typical problem in finite elements [*Wallace and Melosh*, 1994]. We follow the method of *Richardson and Reding* [1991] by separately calculating the outward traction from the overburden equation (9) and applying it to the faces of the lithospheric elements. Since the horizontal deviatoric stress in this approach is determined only up to an arbitrary constant, we set the constant such that deviatoric stresses are minimized by subtracting the global average value from each element.

[29] We consider two different lithospheric density models. In the first model (TD0) we use topography, crustal thickness and density structure as given by Crust 2.0 (G. Laske et al., 2002, available at http://mahi.ucsd.edu/Gabi/rem.html). For the subcrustal lithosphere, we take into account the thickening of the oceanic lithosphere with age according to a half-space cooling model [*Fowler*, 1990] and the isochrons of *Müller et al.* [1994]. In continental regions, we assume that the crust is underlain by lithospheric mantle with a uniform density of 3300 kg m^{-3}. In this model, oceanic regions are close to isostatic equilibrium, while continental regions have, on average, lower elevation than would be predicted by isostasy (Figure 8). The resulting GPE of model TD0 is shown in Figure 9 (top).

[30] In the second model (TD5) we replace the crustal density from Crust 2.0 in continental regions with a value that imposes isostatic equilibrium using Pratt compensation. The results are shown in Figure 9 (bottom). We chose a reference column at a mid-ocean ridge from Crust 2.0. The column, of thickness D = 100 km, and mass M consists of 2.57 km of seawater of density 1020 kg m^{-3}, a 6.6 km thick crust of density 2880 kg m^{-3} and 90.9 km of mantle of density 3300 kg m^{-3}. The crustal density in the continents is then given by $\rho_c = [M - \rho_m(D + h' - C)]/C$, where C is the crustal thickness from Crust 2.0 and h' is the elevation less the contribution from dynamic topography as computed from model SLB. The dynamic topography must be subtracted from the actual elevation because it is a nonisostatic component of topography. Dynamic topography is not subtracted for TD0, since no assumptions are being made regarding the origin of topography. We note that subtraction of dynamic topography, while model-dependent, has small effects on computed values of ρ_c and the resulting stress field. Oceanic regions and the subcrustal lithosphere are treated identically in both TD0 and TD5.

[31] There are two possible reasons that model TD0 deviates from isostatic equilibrium: (1) crustal and lithospheric structure that is still uncertain under continents, particularly the density of the lower crust and the mantle

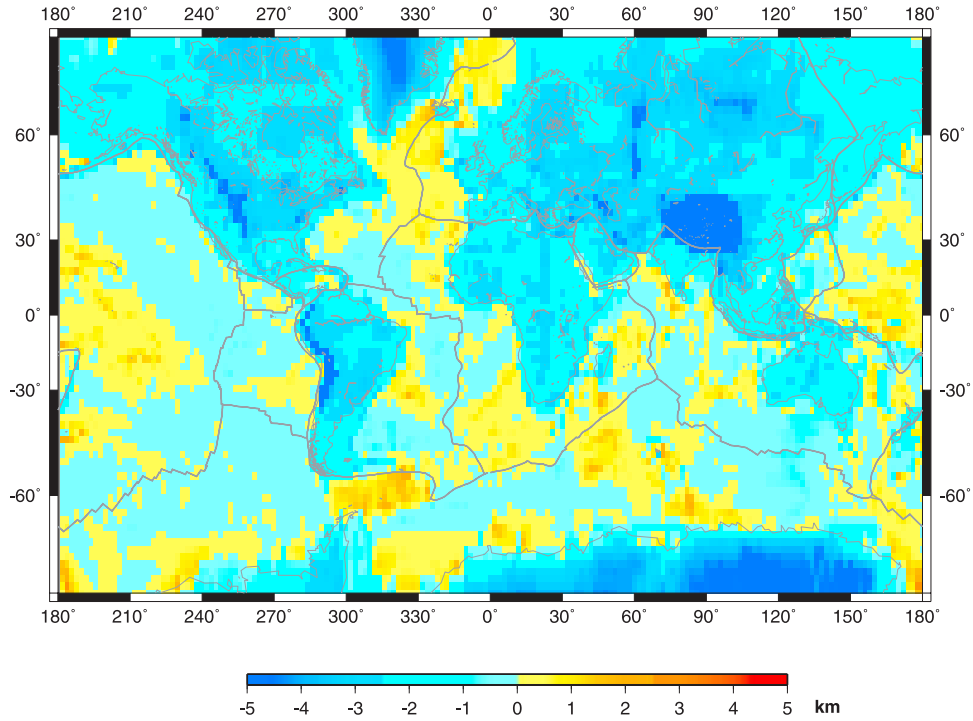

Figure 8. Residual topography using elevations, crustal thickness, and density profiles from Crust 2.0 and the assumption of isostasy. Mantle density is 3300 kg/m^3. Positive areas have an actual elevation higher than determined by isostasy; negative areas have a lower elevation than determined from isostasy.

portion of the lithosphere [*Fischer*, 2002] and (2) contributions to topography that are dynamically, rather than isostatically supported [*Cazenave et al.*, 1989; *Colin and Fleitout*, 1990; *Le Stunff and Ricard*, 1995]. Model TD5 is an idealization from which the real Earth certainly deviates. The extent of the deviation from isostasy, however, is difficult to determine because of poor constraints on lower crustal density structure, and dynamic and flexural contributions to topography. By using two end-member models we hope to bracket the possible resulting stresses. Previous studies have used approaches that are similar to one of these two end-members. As in our model TD0, *Bai et al.* [1992] and *Richardson and Reding* [1991] used estimates of crustal thickness from seismic studies, but with a constant density. As in model TD5, isostatic compensation was used to constrain density structure by *Jones et al.* [1996], *Bird* [1998], *Flesch et al.* [2000], and *Steinberger et al.* [2001], though Airy compensation was assumed in these models.

5. Results

5.1. Mantle Contributions

[32] Model SLB is characterized by very long wavelength (~degree 2) variations in regime and azimuth (Figure 10 (SLBH); Figure 11 (SLBDT), and Figure 12 (SLB = SLBH + SLBDT). For example, nearly all of North America shows a strike-slip regime with ENE to NNW compression, with the azimuth of the most compressive horizontal stress ($\tau_{H\max}$) varying smoothly from southwest to northeast. This is particularly evident when looking only at the horizontal tractions (SLBH) in Figure 10. The global pattern is dominated by centers of thrust regime in the western Pacific and Southeast Asia and in the vicinity of Panama. Compression in these regions is produced by the strongly convergent mantle flow and downwelling in model SLB (Figure 7), which produces directions of maximum compression normal to the strike of current and past subduction. In the northwest Pacific compressive stresses of nearly 200 MPa are generated in the direction of subduction. In North America, compressive stresses are generated by the convergent flow due to the subduction of the former Farallon plate. In South America the pattern of stresses is similar to other subduction zones, but the magnitudes are greatly reduced as the buoyancy available to drive flow is much smaller compared to North America and the northwest Pacific.

[33] As mantle flow in the SLB model is driven exclusively by subducted buoyancy, shear stresses away from subduction zones are the result of passive upwelling return flow, concentrated primarily in the central Pacific and Atlantic basins. In both basins, except for the northern Atlantic and parts of the eastern Pacific extensional stresses are largely oriented E-W, which agrees with the rifting of the African continent. Extension is also prominent in the eastern Atlantic, but does not extend into the continental portions of North and South America. Interestingly at most mid-ocean ridges $\tau_{H\max}$ is normal to their strike, which is due to the high resisting tractions at the plate boundary, as seen in Figure 7.

[34] Examining separately the contributions to the stress field due to horizontal and radial tractions, we see that the horizontal component of the mantle tractions generates an almost pure strike-slip stress regime: principal stresses are nearly equal in magnitude but opposite in sign (Figure 10).

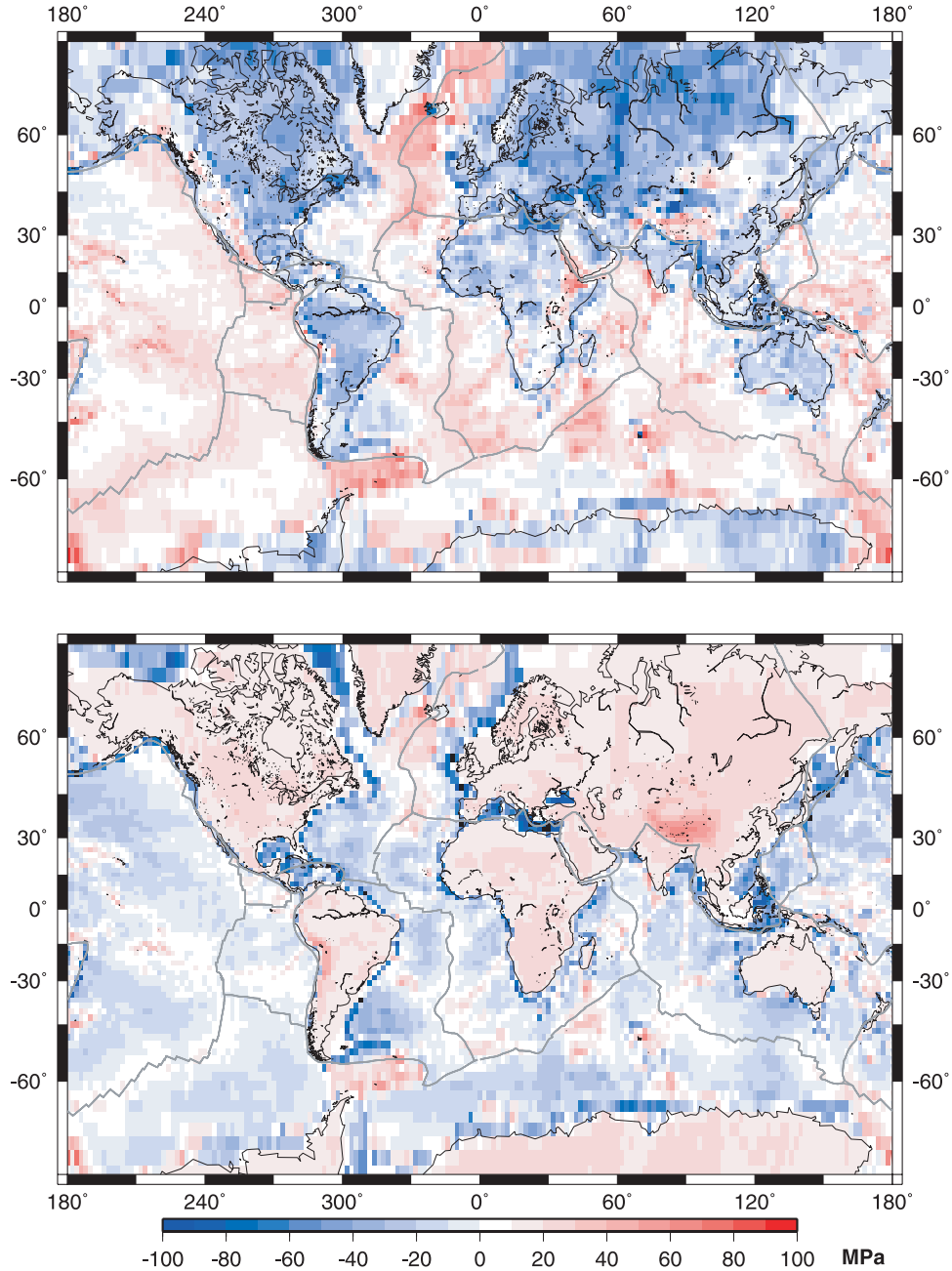

Figure 9. Mean outward traction Ω/H (10) from topography and density loads: (top) TD0 and (bottom) TD5.

This initially surprising result is easily understood when looking at the thin shell equations (5a), which require that the principal stresses be equal and opposite when radial tractions are zero. The small deviations from a strike-slip regime may be due to the deformation of the shell in regions of strong convergence and divergence in the full finite element calculation, which does not use the thin shell approximation.

[35] Radial mantle tractions yield two distinct contributions: membrane stresses that are isotropic, and gravitational stresses (Figure 11). The isotropy of the membrane stresses leads to extension in regions of elevated dynamic topography and compression in dynamic basins, with maximum values of 50–60 MPa. Radial tractions tend to produce extension in the vicinity of ridges, although the direction of extension we predict is parallel rather than perpendicular to the ridges. Extension is also predicted in the mid-Pacific, southern and eastern Africa and eastern Europe. The largest stresses, which are compressive, are around the trenches of the west Pacific and East Asia, the result of recent and past subduction. Because membrane stresses are isotropic, they do not affect the orientation of the stress tensor, although they do influence the regime. The stress pattern due to gravitational potential is a little more complex, with stresses showing more of a strike-slip character and with well defined maximum compressive principal stress directions

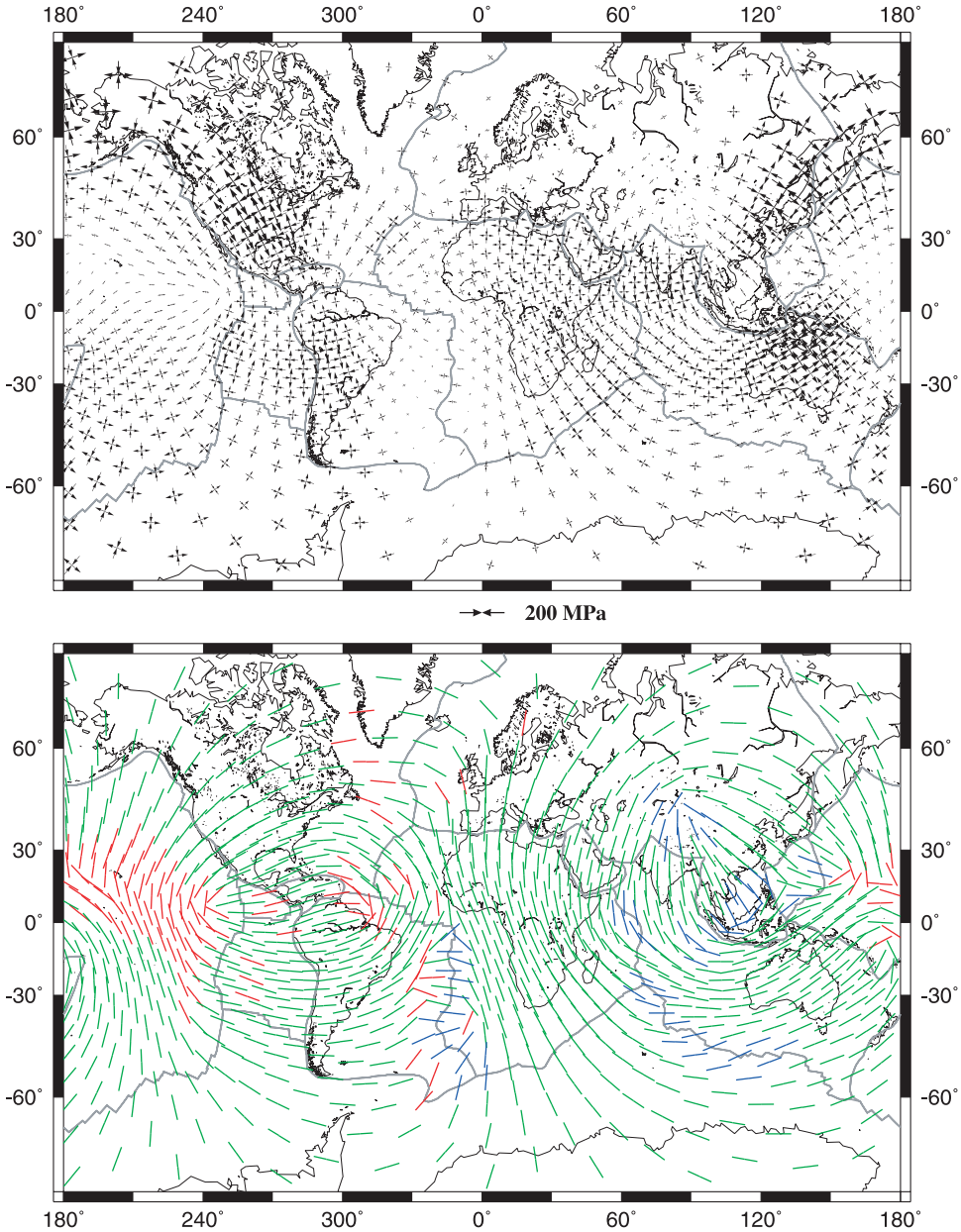

Figure 10. Predicted stresses for only the horizontal tractions of model SLB. (top) Principal directions of stress, indicated by arrows. Outward directed arrows indicate tension, inward directed arrows indicate compression, and the length of the arrow is proportional to the magnitude. Regions of strike-slip behavior appear as one compressional and one tensional pair of arrows. The longest compressional arrow, or shortest tensional arrow in regions of pure tension indicates the direction of maximum compressive principal stress ($\tau_{H\max}$), the direction that is plotted on the WSM. We show only every third point for clarity ($6^\circ \times 6^\circ$ at the equator). (bottom) Direction of the most compressive horizontal stress, with orientation indicated by lines. Red indicates a normal stress regime, green indicates strike slip, and blue indicates thrust. The regime determination follows *Simpson* [1997]. The length of the lines in Figure 10 (bottom) does not contain magnitude information.

(Figure 11a) and maximum compressive stress values that are not necessarily centered over areas of highest or lowest topography as in the case of membrane stresses (Figure 11b). For instance, the high stresses in North America are a result of the high topography in the Pacific and Atlantic basins pushing toward the continent and the low topography in the Bering Sea and Columbia pulling away from the continent. This also results in a NE-SW $\tau_{H\max}$ direction and a least compressive horizontal stress ($\tau_{H\min}$) that is extensional. Overall, these stresses are higher than the membrane stresses with maximum values of 120–130 MPa, though most are in the 50–60 MPa range. The pattern generated by the gravitational contribution of the radial tractions is strikingly similar to that of the horizontal tractions described

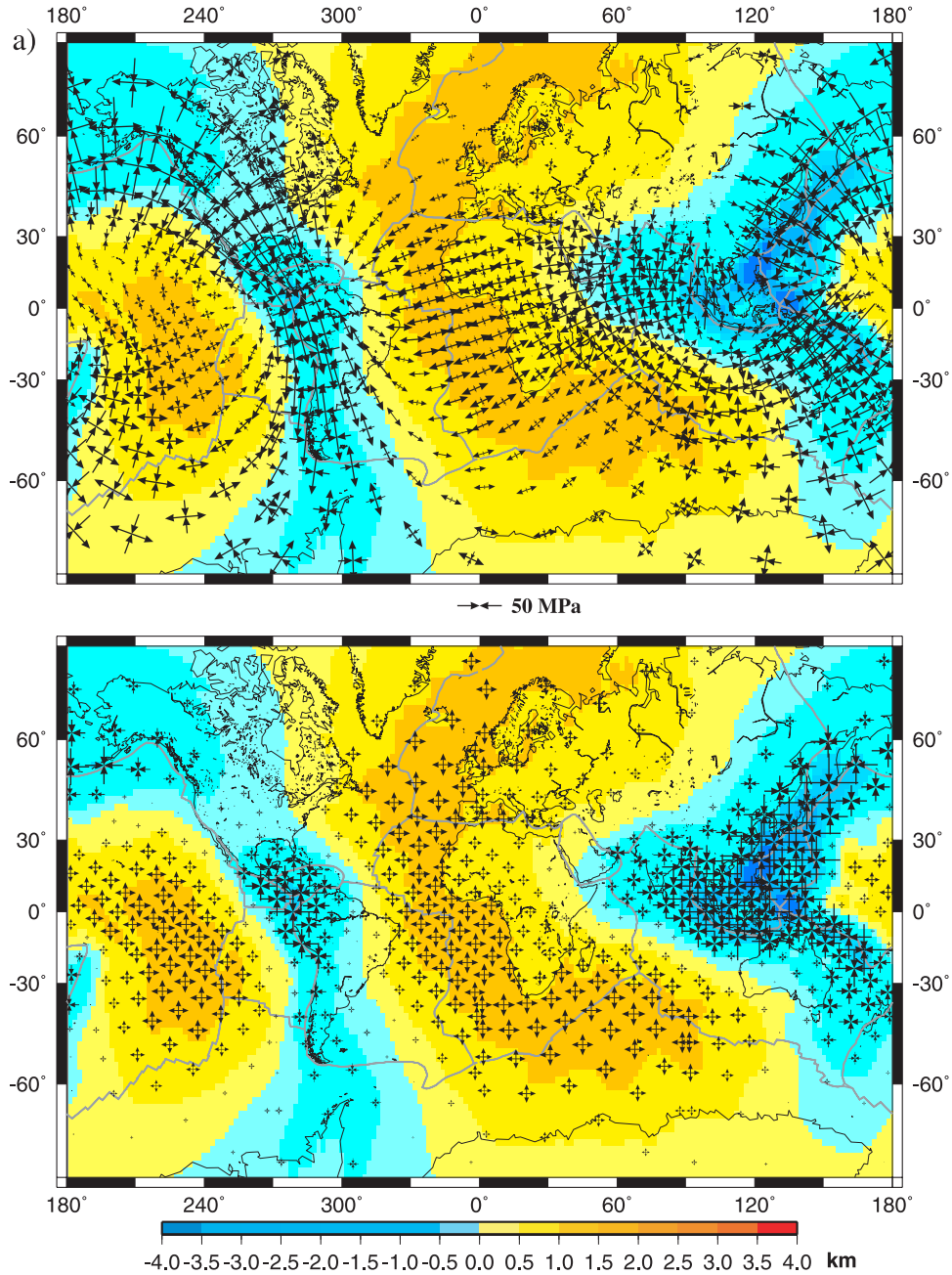

Figure 11. (a) Stress due to dynamic topography computed with model SLB: (top) from gravity sliding and (bottom) from membrane deformation, with the corresponding relief in km. (b) Combined dynamic topography stresses for model SLB. Note difference in scale from Figure 10.

above (Figure 10), although smaller in magnitude. This similarity can be explained by the purely poloidal nature of the mantle flow: regions of downwelling and therefore dynamical downward deflection of the lithosphere are also regions of horizontally convergent flow.

[36] When combined with the horizontal tractions, radial tractions have two notable effects. First, their addition generates an extensional regime at ridges, although the orientation of $\tau_{H\max}$ is opposite to observations. Second, there is an increase in the magnitude of extension in Africa and the magnitude of compression in southeastern Asia (Figure 12).

[37] Model LVC shows that the main effect of the low-viscosity channel is to reduce the connection of deeper flow with the surface, which reduces the basal tractions (Figure 13). This reduction is much greater for horizontal than for radial tractions; in LVC horizontal stresses are ~60% less than for SLB, but LVC radial membrane stresses are only ~20% less than SLB. As a result, in regions of large dynamic topography, such as southeast Asia and the western Pacific, the radial contribution is comparable to that of horizontal tractions and therefore the stress regime is no longer predominantly strike slip in character. For other regions the orientation and character of the stresses of

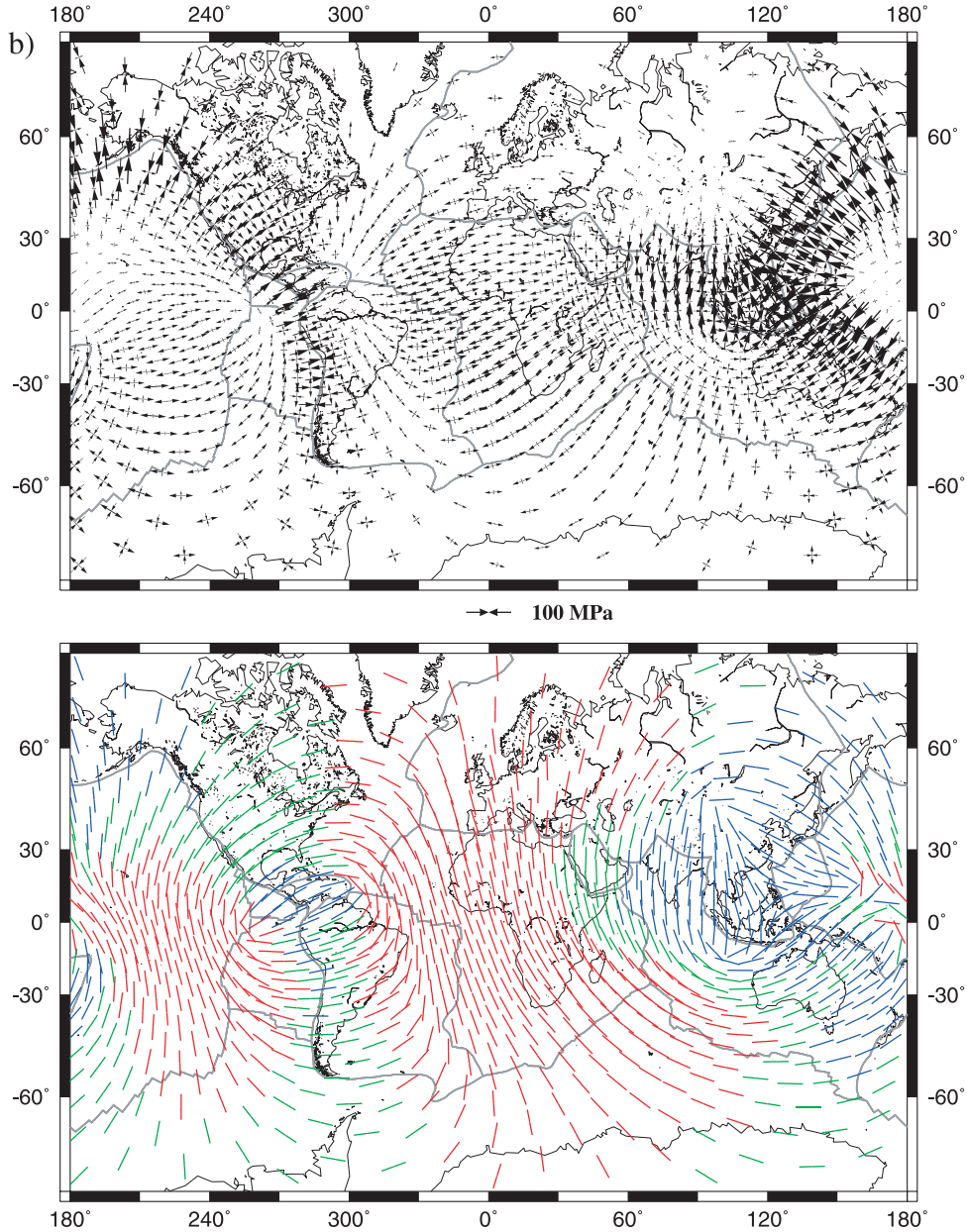

Figure 11. (continued)

LVC are very similar those of SLB, although smaller in amplitude.

[38] The existence of plates is a manifestation of large lateral rheological variations in the plate-mantle system. We illustrate the first order influence of such variations by constructing a model that is identical to LVC but for the presence of weak plate boundaries (Figure 14). In this model, elements along plate boundaries are assigned a Young's modulus (10^9 Pa) that is two orders of magnitude less than that of the rest of the lithosphere. The most obvious effect of weak plate boundaries is a decrease in the stress magnitudes at plate boundaries and a corresponding increase in stress magnitude in the areas immediately adjacent to plate boundaries. There is some slight change in the $\tau_{H\max}$ directions near plate boundaries, but in general the pattern is the same as when weak plate boundaries are not considered. This result is similar to that of *Yoshida et al.* [2001]. This result also supports our contention that the stress field is not unduly sensitive to those aspects of the force balance at plate boundaries that may depend on our choice of maximum harmonic degree.

[39] Different approximations to the mantle density heterogeneity field produce different stress fields, as illustrated by model TMG (Figure 15). Given the small anomalies in the tomographic model of *Grand et al.* [1997] the predicted stress amplitudes are smaller than those for SLB, although slightly higher than for LVC. Strong, ENE-WSW trending compression is predicted from far northern Canada, through the eastern United States and Caribbean, down to the western portion of the South American plate, with a greater component of NNW-SSE extension in the United States. The ENE-WSW compression is likely related to the strong

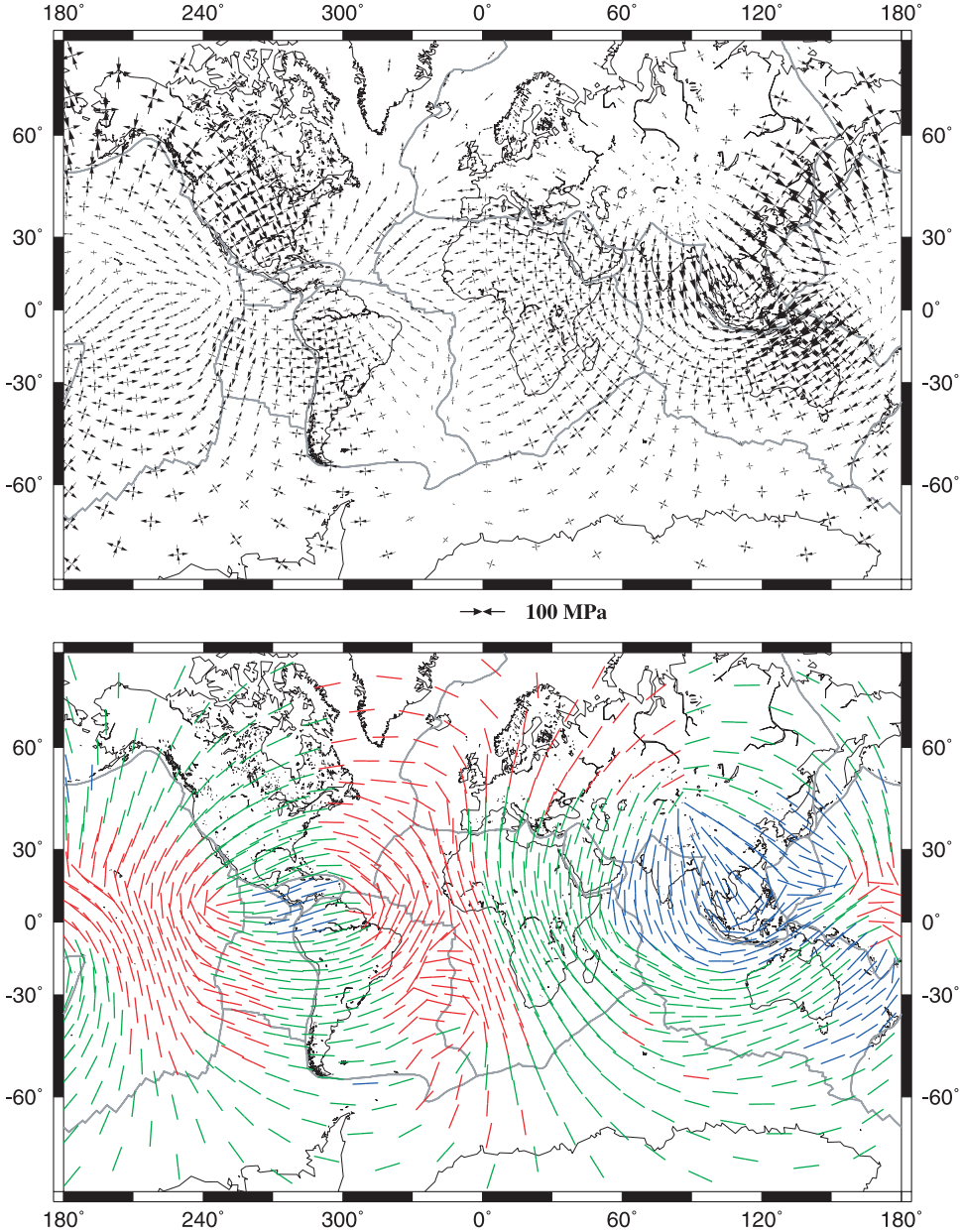

Figure 12. Stresses due to all mantle tractions for model SLB. Symbols are as in Figure 10.

high-velocity anomaly in these regions that has been identified with the remnant Farallon slab [*Grand et al.*, 1997]. The western United States is in slight tension or compression. Extension trending N-S is produced for the Cocos and Nazca plates, due to an area of low density beneath the east Pacific ridge, which also causes tension over much of the Pacific plate, with $\tau_{H\max}$ trending toward the area of upwelling. In general, there is tension at ridges, though the direction is variable depending on the local flow. The stress directions at ridges are in better agreement with observations than SLB and LVC, for two main reasons. First, the presence of prominent low-velocity anomalies under the Atlantic and Pacific basin in Grand's model generates active upwellings that give rise to stronger driving tractions at ridges than in the subduction history model. Second, the large-scale upwellings generate larger positive dynamic topography, which contributes to the stress orientations observed here. Except for a small part of eastern Africa, the continent is largely in compression or a strike-slip stress regime, with NW-SE trending $\tau_{H\max}$. The oceanic part of the plate is in tension. Europe is in compression, with $\tau_{H\max}$ changing from NE-SW in the north to NW-SE in the south.

5.2. Lithospheric Contributions

[40] Models TD0 (Figure 16a) and TD5 (Figure 16b) are very different from any of the mantle models. Stress magnitudes for both lithospheric models are less than 100 MPa: maximum values are 45 MPa for TD0 and 80 MPa for TD5. Most values fall between 0–25 MPa for TD0 and 0–35 MPa for TD5. Variations in azimuth and regime occur over much shorter length scales, reflecting the

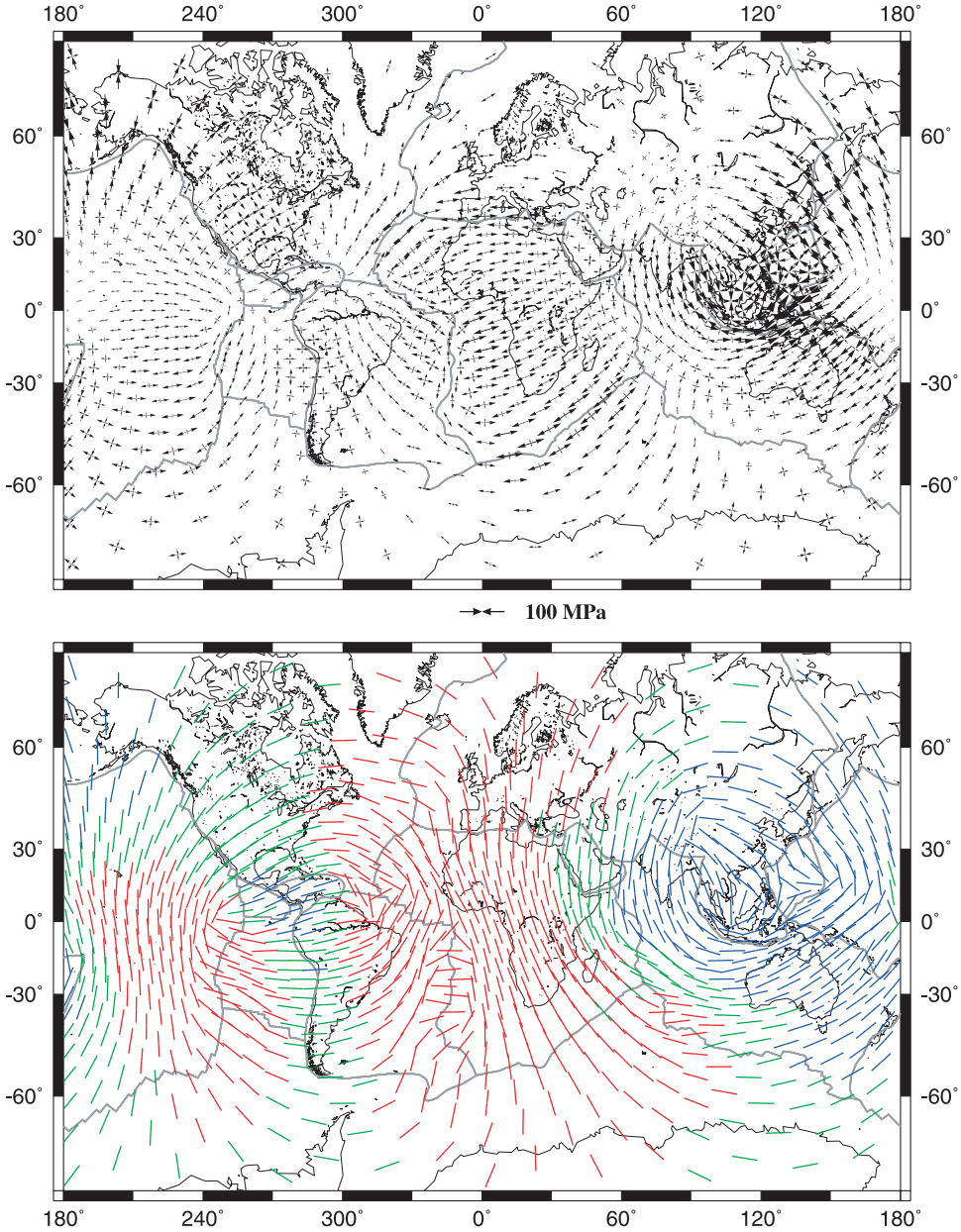

Figure 13. Stresses due to all mantle tractions for model LVC. Note that the scale is half that of Figure 12 (SLB mantle tractions). Symbols are as in Figure 10.

comparatively rapid spatial variability of crustal as opposed to mantle structure. Transitions from dominantly normal to dominantly thrust regimes over length scales less than 600 km are common, for example between the North American Cordillera and the plain immediately to the east. These rapid spatial variations generally reflect those in the pattern of mean outward traction (Figure 9). For example, areas that exert an outward mean traction on their surroundings typically exhibit a normal stress regime, even if they are relatively small in extent such as Tibet, the North American Cordillera, and the high Andes in both TD0 and TD5. It is important to recognize however, that because ours is a global model, with no artificially imposed boundary conditions, topographic stresses may be transmitted great distances and across plate boundaries. While plate boundaries may represent areas where shear stresses are reduced from one plate to another, they will not affect the transmission of stresses from topography. The component of the traction normal to the plate boundary is continuous, and hence lateral forces due to topography and density may be transmitted smoothly.

[41] Lithospheric contributions to the stress field depend strongly on the assumed crustal model. The differences between models TD0 and TD5 are well illustrated by examining lateral variations in the mean outward traction exerted (Figure 9). In model TD5 the assumption of isostatic equilibrium means that the mean outward traction closely mirrors topography. Hence continents have a large outward pressure that leads to a stress regime that is dominantly extensional, while ocean basins are dominantly

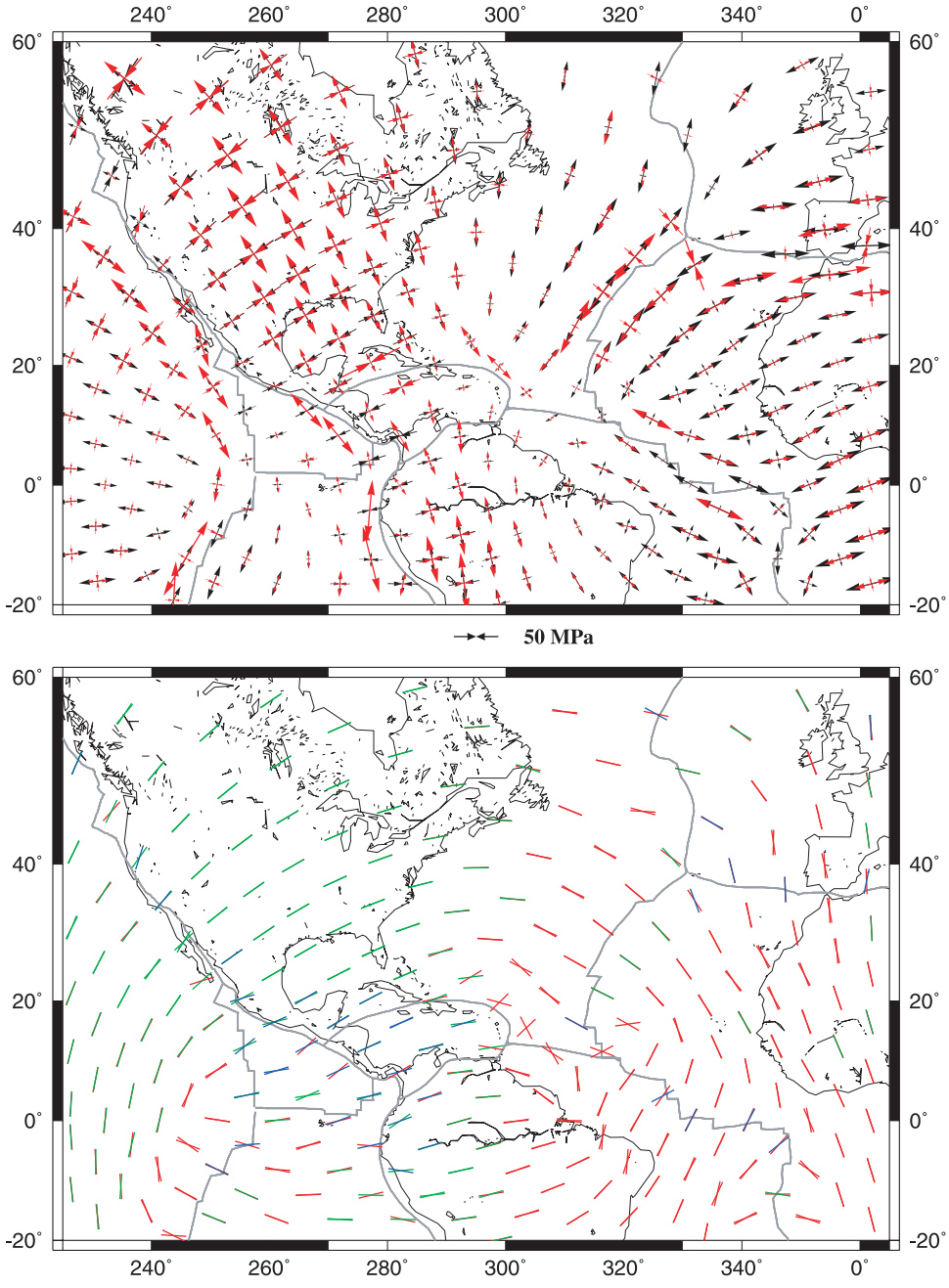

Figure 14. Comparison of stresses with and without weak plate boundaries for the North American region. Weak elements have a Young's modulus 2 orders of magnitude less than the other elements. Red arrows are results with weak plate boundaries; black arrows are results without them. Their near coincidence shows the small influence of weak plate boundaries on the resulting stress orientations. Symbols are as in Figure 10.

in compression. Results for model TD0 differ from TD5 because Crust 2.0 does not enforce isostatic compensation. In TD0, continents are predominantly in compression and much of the ocean basins are in extension (Figure 16a). Differences between TD0 and TD5 are particularly large in tectonically quiet regions where crustal thicknesses may vary greatly for relatively constant elevation. This observation was made by *Fischer* [2002], who found that old mountains typically retain thick crustal roots despite millions of years of unroofing. In neither lithospheric model do the regions of highest stress coincide with tectonic regions that are currently active.

[42] For model TD0 $\tau_{H\min}$ is predominantly normal to the ridge; the regime varies from normal to strike slip. The continent-ocean density difference causes oceanic crust at stable continental margins predominantly to show $\tau_{H\max}$ normal to the margin and a thrust regime. In the interior of oceans, topography can change the overall pattern significantly. For instance, the Rio Grande rise east of South America disrupts the typically compressive stress pattern in

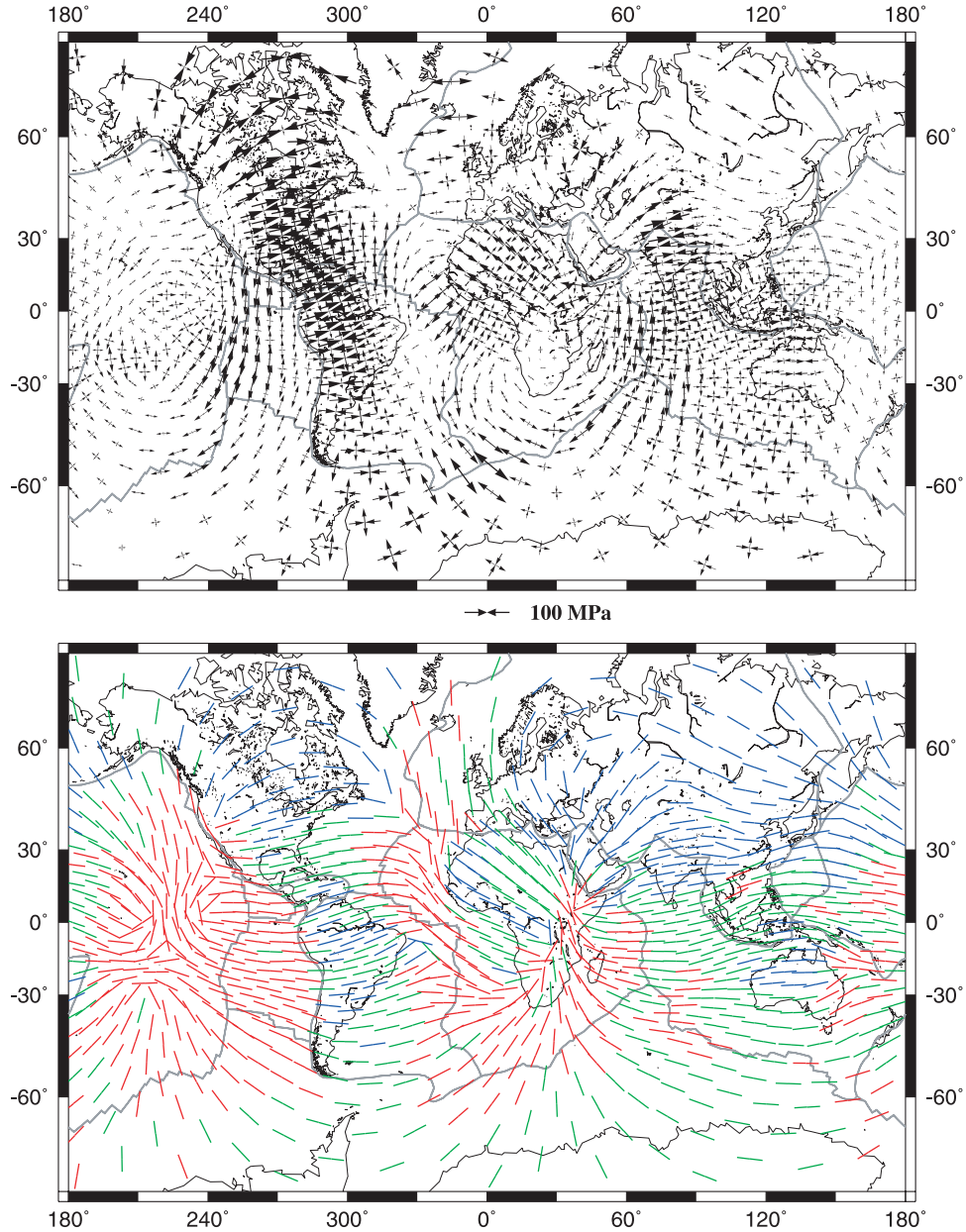

Figure 15. Stresses due to all mantle tractions for model TMG. Symbols are as in Figure 10.

the ocean and creates regions of extension and small stress magnitude. Continents predominantly show thrust or strike-slip regime. In much of North America, average crustal thicknesses and low elevation cause this region to be squeezed between the gravitational potential highs of the Mid-Atlantic Ridge and the Cordillera. South America shows a similar pattern. Stress magnitudes and directions may vary considerably depending on the local crustal structure. For example, in China, the Tarim basin creates an area of very strong compression in a region of predominant extension and minor compression.

[43] Model TD5 predicts extension in Alaska and eastern North America. In central and western North America $\tau_{H\max}$ has a greater northward component compared to TD0. In Europe, $\tau_{H\max}$ is oriented more eastward and most of Africa is in tension instead of just the rift zone. Regions near ridges are more in compression than in TD0. In Southeast Asia the stress varies from ENE-WSW extension to nearly N-S compression at the Java subduction zone. The highest stress levels for TD5 are a result of the continent to ocean transitions.

5.3. Combined Model

[44] The lithospheric stress field is a combination of mantle and crustal contributions. In our model the stresses due to mantle flow are on average a factor of 2–4 greater than stresses due to lithospheric heterogeneity. As a result the contribution from mantle loads dominates the total stress field (Figure 17). In many regions the two contributions to the stress field add constructively. This is not surprising because continental geology and mantle flow are correlated: subduction of the Farallon plate gave rise to the Rockies and

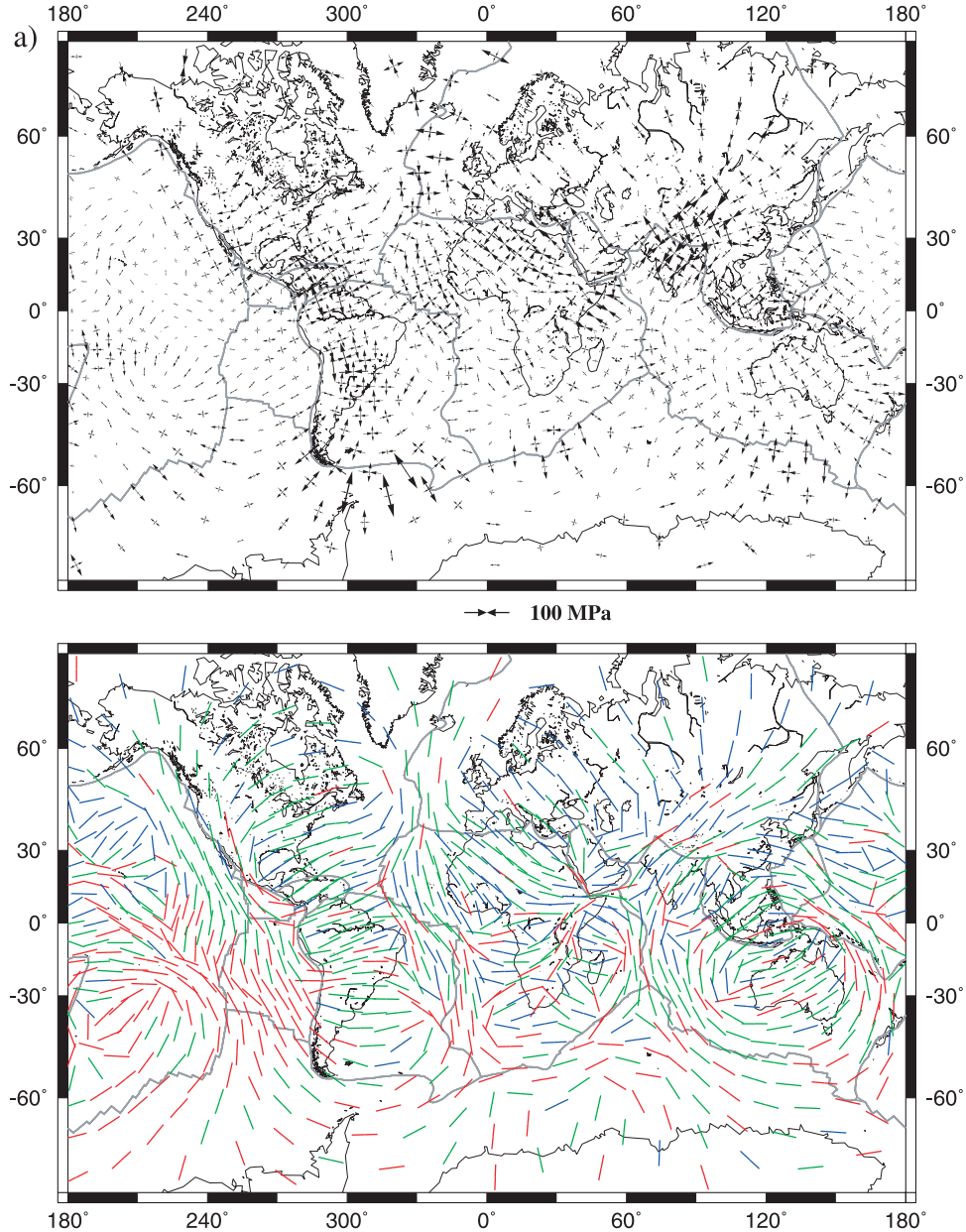

Figure 16. (a) Stresses for model TD0. Topography and density loads are based on Crust 2.0 crustal structure. Oceanic lithosphere thickness and density are determined from a half-space cooling model. (b) Stress results for TD5. Topography and crustal depth are based on Crust 2.0, but continental density is determined from isostatic equilibrium. Oceanic lithosphere thickness and density are determined from a half-space cooling model. Symbols are as in Figure 10.

the Andes, and to persistent downwellings under the Americas [e.g., *Bird*, 1988; *Grand et al.*, 1997]. Western North America is in a strike-slip regime with NE-SW compression, due to the subducted Farallon plate, which causes flow toward the center of the continent. These compressive stresses are reduced slightly by the density difference between North America and the eastern Pacific that results in NW-SE tension. In eastern North America ridge-push from the Atlantic augments the NE compressive stresses generated by the Farallon plate and also generates NW-SE tension of nearly equal magnitude. The most notable effect of adding the crustal contributions to the mantle models is intensification of compressive stresses in Southeast Asia and North America, and of extensional stresses in Africa.

6. Discussion

[45] We compare our results to observations of the state of stress in the crust as summarized by the Word Stress Map [*Zoback*, 1992; B. Müller et al., The 2000 release of the World Stress Map, 2000, available at http://www.world-stress-map.org]. This database is primarily a compendium of measured principal horizontal stress directions, based mainly on earthquake focal mechanisms and borehole

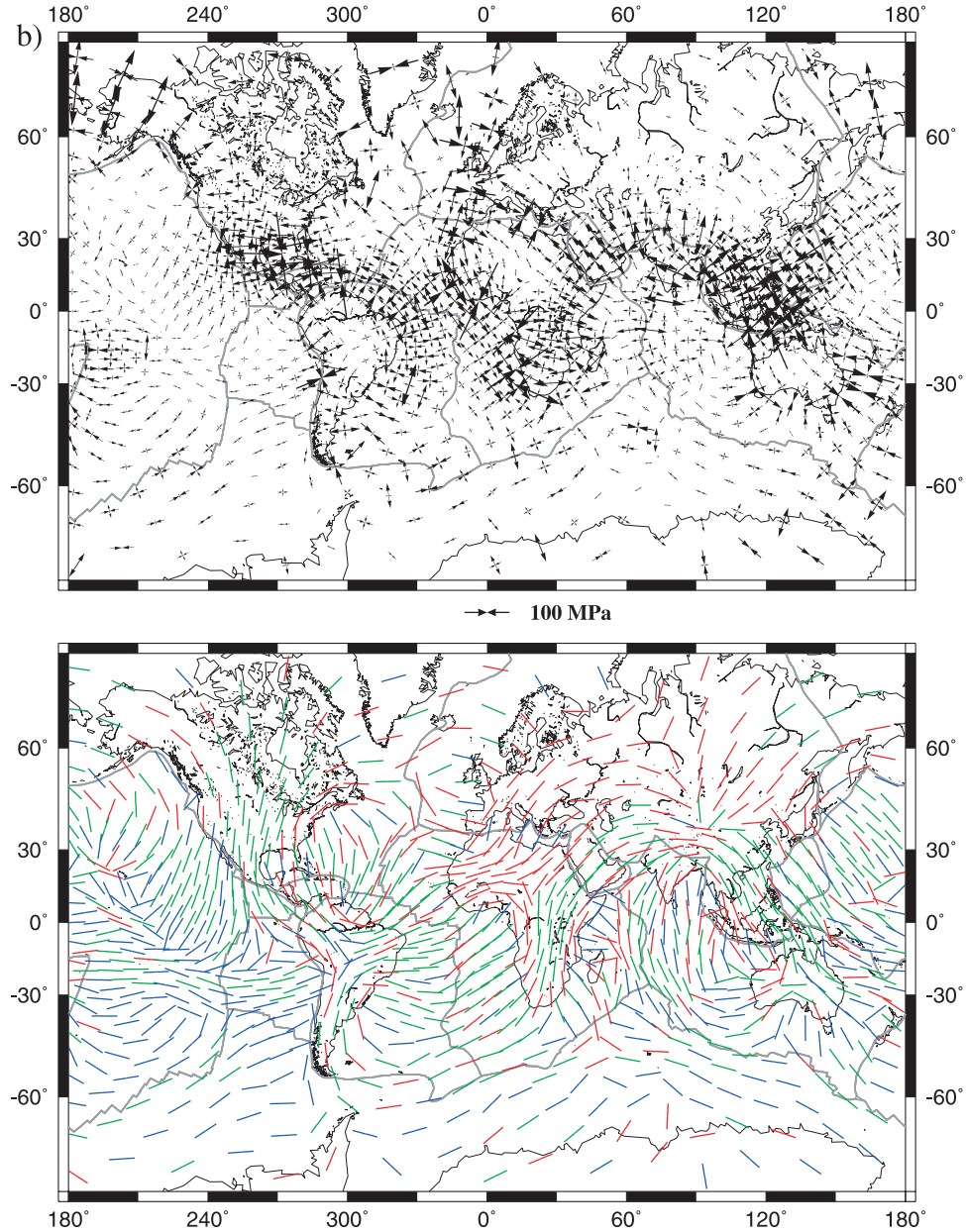

Figure 16. (continued)

breakout data, supplemented by hydrofracturing and overcoring techniques, Quaternary fault slip directions and alignment of Quaternary volcanic vent and dike swarms.

[46] The comparison is not straightforward for a number of reasons. First, measurements of the magnitude of crustal stresses are rare. Earthquake stress drops represent only a lower bound on the magnitude of the nonhydrostatic stress since the earthquake may not completely relax the stress field. Typical stress drops are on the order of 1–10 MPa, with some values as high as 100 MPa [*Ruff*, 2002]. Hydrofracture measurements, which provide magnitude data, have only been completed for a limited number of boreholes. A summary of borehole data [*Townend and Zoback*, 2000] shows that differential stresses vary linearly from around 40–60 MPa at 2 km to around 150 MPa at 8 km and appear to follow the Coulomb friction-failure criteria.

[47] Information on the sense and orientation of the stress regime may not be obtainable from all types of measurements. For example, borehole breakout data measure only the direction of the least compressive stress. In the analysis of many types of observations, it is generally assumed that the vertical stress is one of the principal stress directions. This assumption is valid as long as local topographic slope or crustal heterogeneity does not significantly disturb the stress state. One study has shown that topography in the Cajon Pass borehole area did not significantly affect the stress results [*Liu and Zoback*, 1992]. In addition, stress measurements may have a large degree of uncertainty in orientation, from 10° to 15° for A quality data to greater than 25° for D quality data, and caution must be exercised in comparing predicted stress directions to those in regions with a small data set.

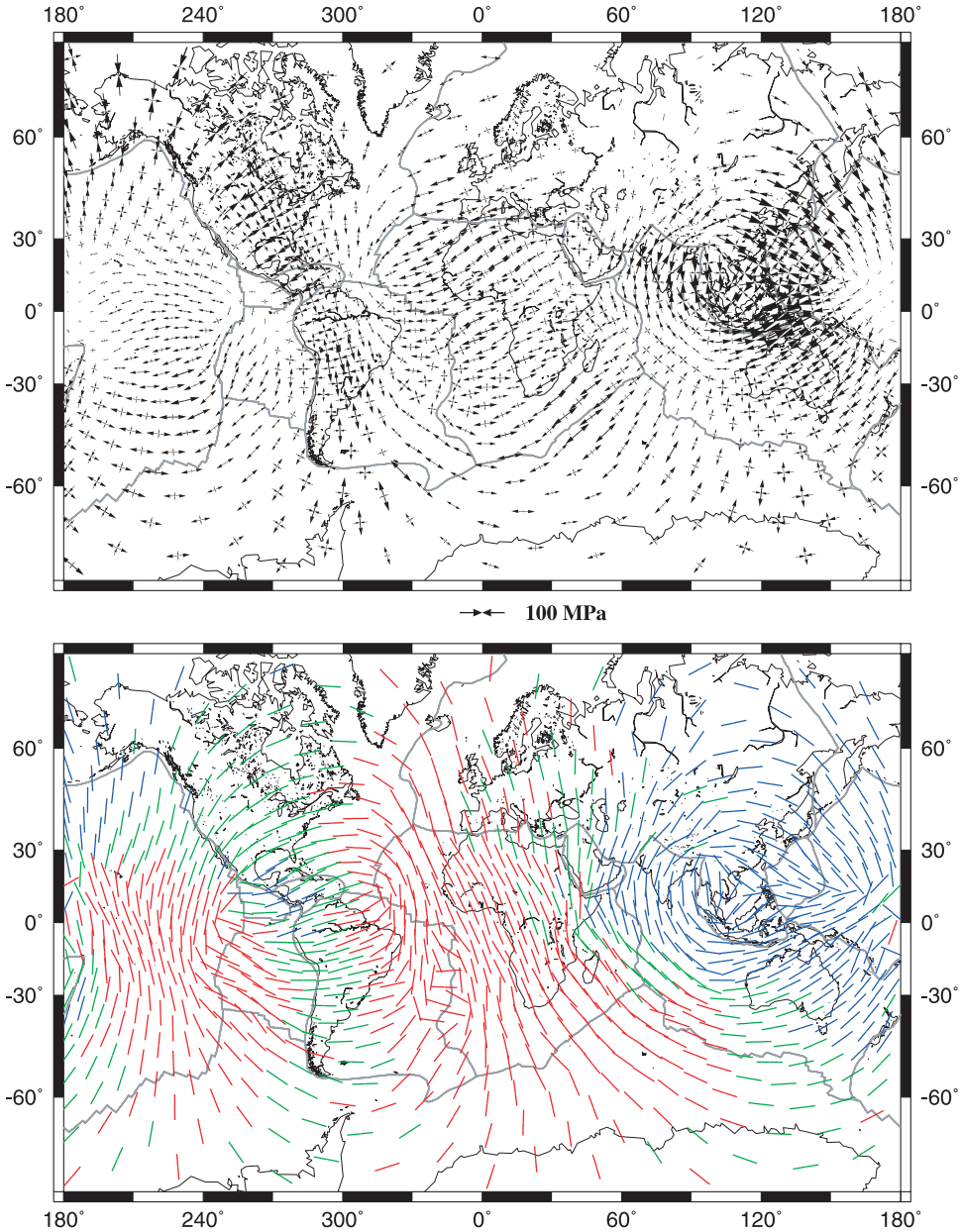

Figure 17. Stresses for model LVC + TD0, which includes all tractions from models LVC and TD0. Symbols are as in Figure 10.

[48] Earthquake focal mechanisms are valuable because they can be used to estimate the orientation (the directions of the three principal stresses) and the sign of the principal components of the stress tensor, so that it is possible to determine whether the stress regime is extensional, compressional, or strike slip. However, earthquake rupture may be influenced by the geometry of preexisting faults and crustal heterogeneity in addition to the prevailing stress regime. Crustal heterogeneity may affect other types of stress determinations as well. Thus *Scholz and Saucier* [1993] argued that stress directions determined in one study were not representative of the state of stress on the San Andreas, but were strongly influenced by a smaller local fault.

[49] Most determinations of stress are based on observations of the upper 20 km of the lithosphere and may not be representative of the state of stress of the lithosphere as a whole. In the vicinity of abrupt lateral variations in topography or crustal structure, the state of stress must vary substantially with depth [*Zoback and Richardson*, 1996]. Indeed, there is observational evidence that the state of stress in the crust may vary strongly with depth: in the Cajon Pass borehole, compressive stress directions averaged over 4 different sections, comprising the bottom 2000 m of the hole, varied over a 50° range [*Zoback and Healy*, 1992]. It has been argued that the data of the World Stress Map may only represent stress in the very top of the crust [*Liu et al.*, 1997] or that stresses may vary with depth due to rheological differences [*Lynch and Richards*, 2001]. Nevertheless, the World Stress Map (Figure 18a) shows regions in which stress directions are consistent over length

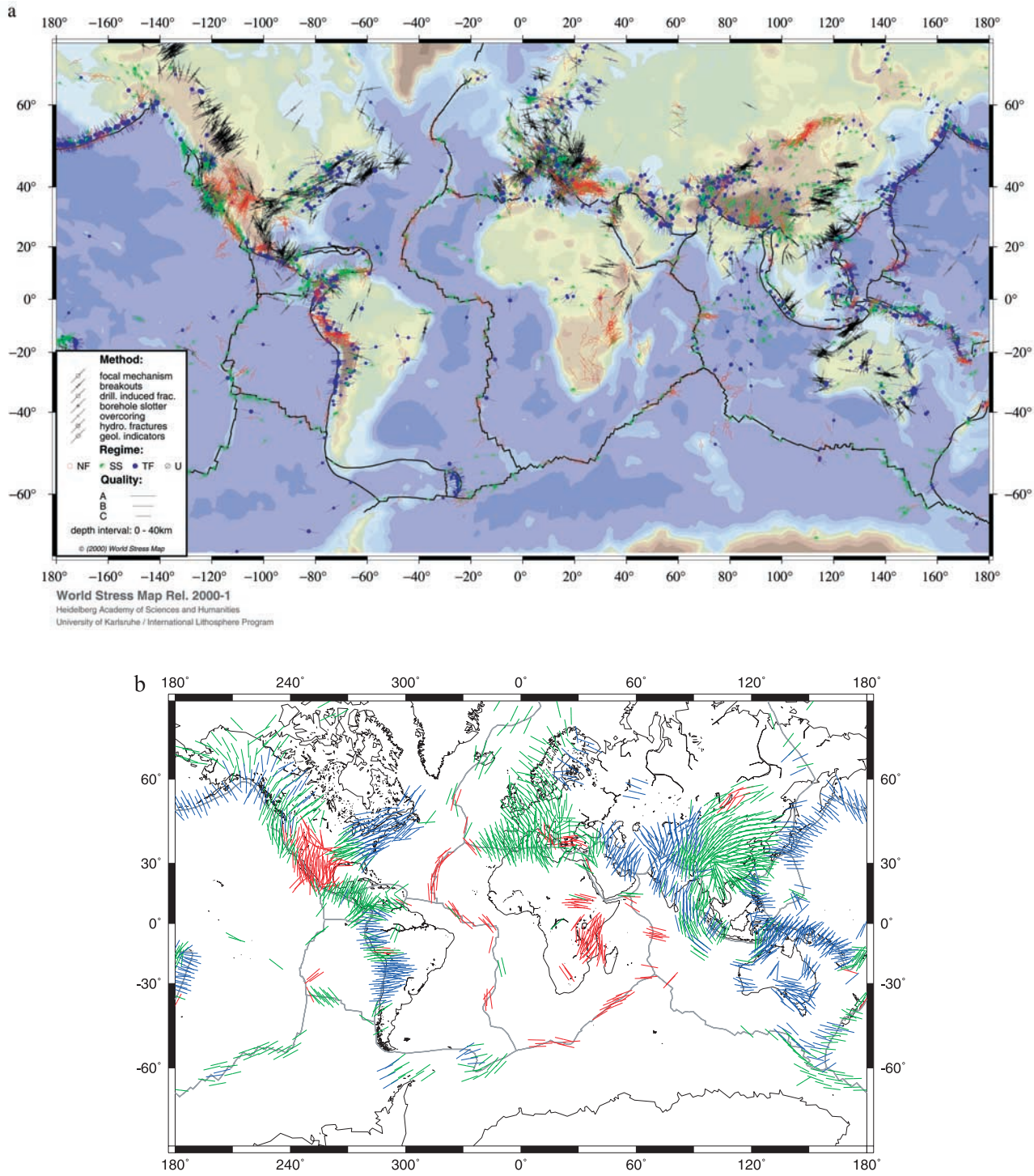

Figure 18. (a) World Stress Map, release 2000. (b) Interpolated WSM using the method of *Bird and Li* [1996] for azimuth information and the method discussed in the text for regime information.

scales that are much larger than the thickness of the lithosphere [*Zoback et al.*, 1989]. In these regions at least, measurements of the shallow stress state may be representative of the lithosphere as a whole.

[50] The definition of quantitative measures of comparison between our model results and the World Stress Map (WSM) is challenging because of the categorical nature of much of the stress observations, the variability of stress measurements in some regions, and the uneven spatial distribution of measurements. We have developed quantitative measures of global fit based on interpolated forms of the WSM data. Because global measures may mask large variations from region to region in the quality of fit, we have also developed a simple ranking system by region.

[51] We have interpolated the azimuth and regime data of the World Stress Map onto our computational grid

(Figure 18b). For the azimuth data, we used the method of *Bird and Li* [1996], based on empirical two-point conditional probabilities, and preclustering of data points that are nearby and similar in azimuth. Interpolation of regime information is more difficult and was not attempted by *Bird and Li* [1996] but is critical in evaluating the relative successes and failures of our models. Rather than empirically determine two-point conditional probabilities from the regime data, we adopted the same probabilities as determined for the azimuth data and used these as a priori weights; we also used the same pattern of preclustering as determined from the azimuth data. While there are no doubt other ways to interpolate the regime data, some of which may be statistically more rigorous, our approach has the advantages of simplicity of implementation and that the relative influence of individual WSM data points upon an interpolated point is identical for azimuth and regime information. In the interpolation, we used the scheme of *Coblentz and Richardson* [1995] to convert the qualitative regime information of the WSM to a quantitative scale.

[52] The result (Figure 18b) is very similar in azimuth to the interpolated map determined by *Bird and Li* [1996]. Following Bird and Li, we consider only those points for which the uncertainty in interpolated azimuth is less than ±45°. These high-quality interpolated values cover 21% of the globe, somewhat greater than the 20% found by *Bird and Li* [1996], a difference that we attribute to the larger number of WSM data now available. The interpolated regimes (N, normal faulting; T, thrust faulting; S, strike-slip faulting) agree remarkably well in all areas with the first order stress patterns as identified by *Zoback* [1992] with the following exceptions: Tibetan Plateau (*Zoback* [1992] finds N versus S/T in our interpolation), mid-African plate (S versus N), and North Africa (T/S versus S). These differences may be due to additions to the WSM database since 1992. In Tibet, examination of the current WSM data reveal N, S, and T regimes in roughly equal abundance, with a tendency toward N regimes closer to the Himalayan front, and T around the southern and northern margins. Interpolation yields T on the margins and S in the interior since no regime type dominates here, which may be considered the best, albeit uncertain, estimate given the current measurements. The mid-African plate in the categorization of *Zoback* [1992] includes western and southern Africa. The number of data in western Africa is too small to determine an interpolated value within our uncertainty bounds, as was the case in the *Bird and Li* [1996] interpolation. Southern Africa in the most recent WSM compilation is dominantly N, but for two S data in southwestern South Africa. Where our uncertainty bounds permit, our interpolated values are all N. North Africa shows mixed regime types, which leads to an interpolated value of S that as in the interior of Tibet can be regarded as an uncertain best estimate.

Table 1. Global Comparison of Models to the Interpolated World Stress Map for Azimuth[a]

	RMS Difference				Variance Reduction			
Model[b]	All	W	Q	QW	All	W	Q	QW
SLBH	49	40	43	38	32	44	43	41
SLBR	53	55	55	55	20	−5	8	−27
SLB	49	40	43	38	32	44	43	41
SLBDT	54	53	57	53	17	2	1	−16
LVCH	48	39	42	36	35	48	46	46
LVCR	53	55	54	56	20	−7	9	−30
LVC	48	38	42	36	35	48	46	46
LVCP	48	39	42	36	34	48	45	47
TMG	50	42	47	40	28	38	32	32
TD0	45	39	38	37	42	47	55	42
TD5	50	45	48	44	27	29	28	20
SLBR + TD0	45	39	39	38	40	46	53	42
SLB + TD0	47	38	40	35	35	50	50	49
LVCR + TD0	45	39	39	38	40	46	53	42
LVC + TD0	45	35	37	32	41	58	58	59
TMG + TD0	48	40	43	38	34	44	43	40

[a]All, all interpolated points from the World Stress Map; W, weighted by the variance of the interpolated point; Q, only those interpolated points that have an uncertainty in azimuth <45°; QW, weighting but including only those points with uncertainty <45°.

[b]First three letters for each model are as defined in the text; subsequent letters have the following meaning: H, only horizontal tractions; R, only membrane stresses from radial tractions; DT,: membrane stresses and gravitational sliding from radial tractions; P,: weak plate boundaries included. Combined models are indicated by addition, e.g., SLB + TD0 combines all mantle tractions from model SLB with all tractions from model TD0.

Table 2. Global Comparison of Models to the Interpolated World Stress Map for Regime[a]

	RMS Difference				Variance Reduction			
Model	All	W	Q	QW	All	W	Q	QW
SLBH	0.42	0.35	0.38	0.35	58	65	71	73
SLBR	0.52	0.52	0.51	0.52	36	22	46	40
SLB	0.46	0.39	0.41	0.40	50	56	66	64
SLBDT	0.46	0.39	0.42	0.43	51	56	64	59
LVCH	0.40	0.30	0.42	0.40	61	75	63	64
LVCR	0.51	0.52	0.50	0.50	38	23	50	44
LVC	0.43	0.36	0.42	0.43	56	63	64	59
LVCP	0.44	0.32	0.49	0.48	55	70	51	48
TMG	0.45	0.46	0.42	0.42	53	39	64	60
TD0	0.51	0.50	0.50	0.49	40	29	50	46
TD5	0.51	0.50	0.54	0.52	38	27	40	39
SLBR + TD0	0.50	0.50	0.46	0.47	41	28	57	51
SLB + TD0	0.46	0.39	0.40	0.41	51	56	67	62
LVCR + TD0	0.49	0.50	0.45	0.46	44	29	59	53
LVC + TD0	0.44	0.37	0.41	0.42	55	60	65	61
TMG + TD0	0.45	0.38	0.43	0.43	52	59	63	59

[a]Definition of quantities and models as in Table 1.

[53] Global comparisons to our finite element calculations are based on root-mean-square differences and variance reductions of azimuth and regime (Tables 1 and 2). The variance (amplitude) of the WSM azimuth data was computed using the proper circular formulae for standard deviation [*Mardia*, 1972]. Regime information was extracted from the finite element calculations using the A_ϕ parameter and regime intervals of *Simpson* [1997]. Finite element and WSM regime information were both expressed on the following numerical scale following *Coblentz and Richardson* [1995]: N = 0, S = 0.5, T = 1.

[54] Regional comparisons are based on semiquantitative scoring of agreement in azimuth and regime in those regions that show a well-defined and uniform stress state (Table 3). The choice of regions is based on that of *Zoback* [1992] with some differences based on our interpolated map. We subdivided the western North American plate into three subregions: (1) Basin and Range and Mexico north of Mexico City, (2) northwest Canada, and (3) Central America. We subdivided the mid-African Plate category

Table 3. Regional Comparison of Different Models to the World Stress Map[a]

Location	TD0	TD5	SLB+TD0	LVC+TD0	TMG+TD0
Mid-North American Plate	+/+	0/–	+/0	+/0	+/+
Basin and Range/Mexico	0/+	+/0	0/0	0/0	+/0
Western Canada	0/+	–/0	+/0	+/0	+/0
Central America	+/+	–/0	+/+	+/0	+/+
South American Plate	+/0	–/+	+/+	+/0	+/0
High Andes	+/+	–/+	+/0	+/0	+/0
Western Europe	+/+	–/0	+/+	+/0	0/0
Iran	–/+	+/0	+/0	+/+	+/+
China/eastern Asia	0/0	0/+	0/+	0/0	+/0
Tibetan Plateau	+/0	–/0	+/0	+/0	0/+
East African Rift	0/+	+/0	0/0	0/+	+/+
Southern Africa	+/+	0/+	+/0	0/+	–/+
Sudan	+/–	0/0	–/0	0/+	–/+
North Africa	+/+	+/0	+/+	+/+	+/+
India	+/+	+/0	+/+	+/+	0/+
Central Indian Ocean	–/–	+/0	+/+	+/+	–/0
West Indian Ocean	–/–	–/0	+/0	0/–	+/+
Central Australia plus NW shelf	+/0	+/–	+/0	+/+	+/+
South coastal Australia	–/0	+/–	–/0	0/0	–/0
Young Pacific Plate	+/0	+/0	+/0	+/0	0/0
Old Pacific Plate	0/+	0/+	+/+	0/+	0/+
Totals	8 + 9 = 17	2 + 3 = +5	15 + 8 = 23	13 + 8 = 21	8 + 12 = 20

[a]Two entries are given separated by a slash: the first refers to agreement in azimuth, the second to agreement in regime. Symbols are assigned as follows for azimuth: disagreement <30° (plus), 30°–60° (0), >60° (minus); and for regime: agreement (plus), partial disagreement: S versus N or S versus T (zero), opposite: T versus N (minus). Totals for azimuth and regime are reported separately for each model, and the sum of azimuth and regime is also given.

of *Zoback* [1992] into (1) southern Africa and (2) Sudan. We excluded the Nazca plate and Antarctica from our analysis given the paucity of measurements in those regions. Finally, we added Iran as a category. Azimuth and regime are evaluated separately and assigned a score of +1 for agreement (<30° difference in azimuth, agreement in predominant regime type); −1 for disagreement (>60° difference in azimuth, perfect disagreement in predominant regime type (T versus N); and 0 for partial disagreement (intermediate differences in azimuth, and in predominant regime type: S versus T or S versus N).

[55] We discuss in detail the combined model of stresses produced by mantle tractions and crustal contributions (LVC + TD0), which overall matches the WSM the best (Figure 19a). This model produces global weighted variance reductions of the high-quality data (QW in Tables 1 and 2) of 59% and 61% in azimuth and regime, respectively. The combined model matches the observations better than either of its components (LVC or TD0) individually (Tables 1–3). Western North America is in a strike-slip regime with NE-SW compression, because of the subducted Farallon plate, which causes flow toward the center of the continent. These compressive stresses are reduced slightly by the density difference between North America and the eastern Pacific that results in NW-SE tension. In eastern North America ridge push from the Atlantic augments the NE compressive stresses generated by the Farallon plate and also generates NW-SE tension of nearly equal magnitude. The predicted stresses agree well in azimuth with the WSM in eastern North America, Canada and Alaska. In the Basin and Range the model predicts NW-SE extension, opposite to most of the observations and regional tectonics. The model predicts the correct stress regime (strike-slip) in southern California and compression oriented near normal to the plate boundary. The model fails to predict the rotation of the $\tau_{H\max}$ direction from NE-SW to N-S observed from eastern seaboard to Mexico. In the Andes the model predicts E-W compression, except for the highest Andes, where topography produces N-S tension, which matches observations. In Europe we predict E-W extension due to the large resisting tractions at the Atlantic ridge (pulling westward) and the large flow toward subduction zones in the east (pulling eastward). The observations however, show no consistent pattern of extension. The model predicts that the entire African plate is under NNE-SSW tension as a result of the resisting tractions at all the ridges pulling away from the continent. Both observations and recent tectonics indicate largely ESE extension in eastern Africa, a 45° rotation from our prediction. Downwelling under eastern Asia leads to strong NW-SE compression in Southeast Asia, Tibet and India. The model predictions match well for southeast China, and the stress regime observed in India, although the directions are off by 30°, but disagree strongly with those in Tibet. Regional models of Eurasia that do not account directly for basal tractions but account indirectly for coupling between plate and mantle, and that account for lateral variation in strength, have better captured the full variation in stress style observed in Tibet [*Flesch et al.*, 2001]. In northeast China and Lake Baikal we predict EW compression, a stress regime opposite to WSM observations. At the Ninety East ridge the model predicts N-S compression, as in the observations. Along the mid-ocean ridges in the region we predict stress directions seemingly opposite to those observed. The distinctive rotation of compressive stress directions from E-W in Australia to N-S near India is well matched by our predicted stresses.

[56] Model SLB + TD0 (Figure 19b) produces global weighted variance reductions of 49% and 62% in azimuth and regime, respectively, and is marginally better than LCV + TD0 in our regional comparison. As with LVC + TD0, SLB + TD0 does not capture the spatial variability of stress regime in many regions, including within the North

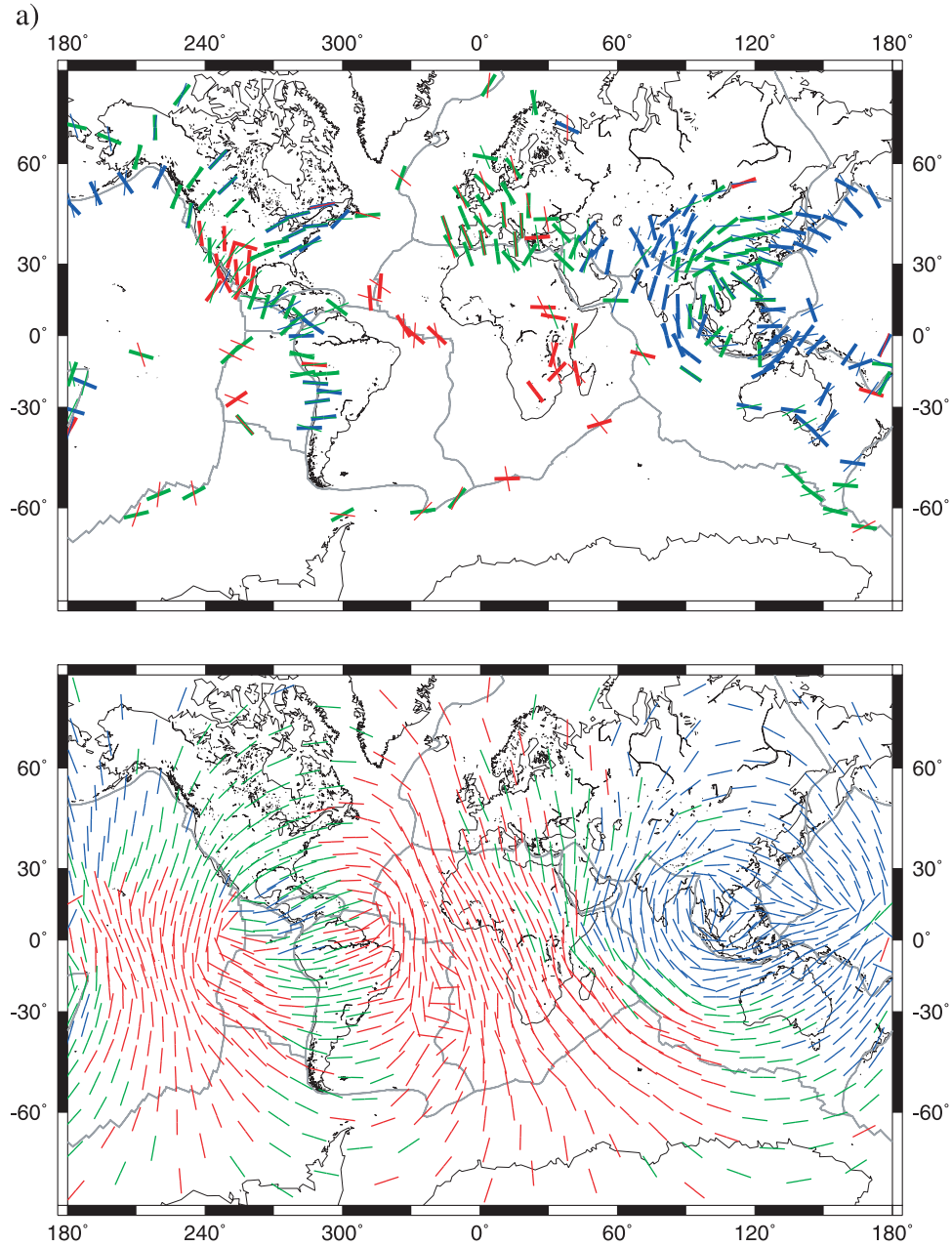

Figure 19. Results of model calculations compared with the World Stress Map. (top) Interpolated World Stress Map values as bold lines and model calculations as thin lines. (bottom) Global computational result. As in previous figures, lines are oriented in the direction of the most compressive horizontal stress. Red indicates a normal stress regime, green indicates strike-slip, and blue indicates thrust. We show only every third point for clarity (6° × 6° at the equator) for (a) LVC + TD0, (b) SLB + TD0, (c) TMG + TD0, (d) TD0, and (e) TD5.

American plate: the model underestimates the amount of compression in the midplate region and northwestern Canada, and the amount of extension in the Basin and Range. In South America, the dominantly E-W azimuth is correctly captured, but the model does not reproduce the presence of normal regime in the high Andes. In Africa, the stress regime is predicted to be uniformly strike slip and so does not capture the extensional regime observed in the East African Rift and southern Africa. In eastern Asia, the model predicts azimuths that are too southerly, although the dominantly strike-slip regime is correctly predicted here, as is compression in India and in the western Indian Ocean. Northwestern Pacific subduction is characterized by trench-normal compression, but southwestern Pacific subduction shows azimuths that are trench parallel in the Tonga-New Zealand plate boundary. The extent of thrusting is overestimated in eastern Asia and in Central America. Comparison with LVC + TD0 shows that the primary effect of the low-viscosity channel is to diminish the magnitude of mantle tractions, particularly horizontal tractions. The result

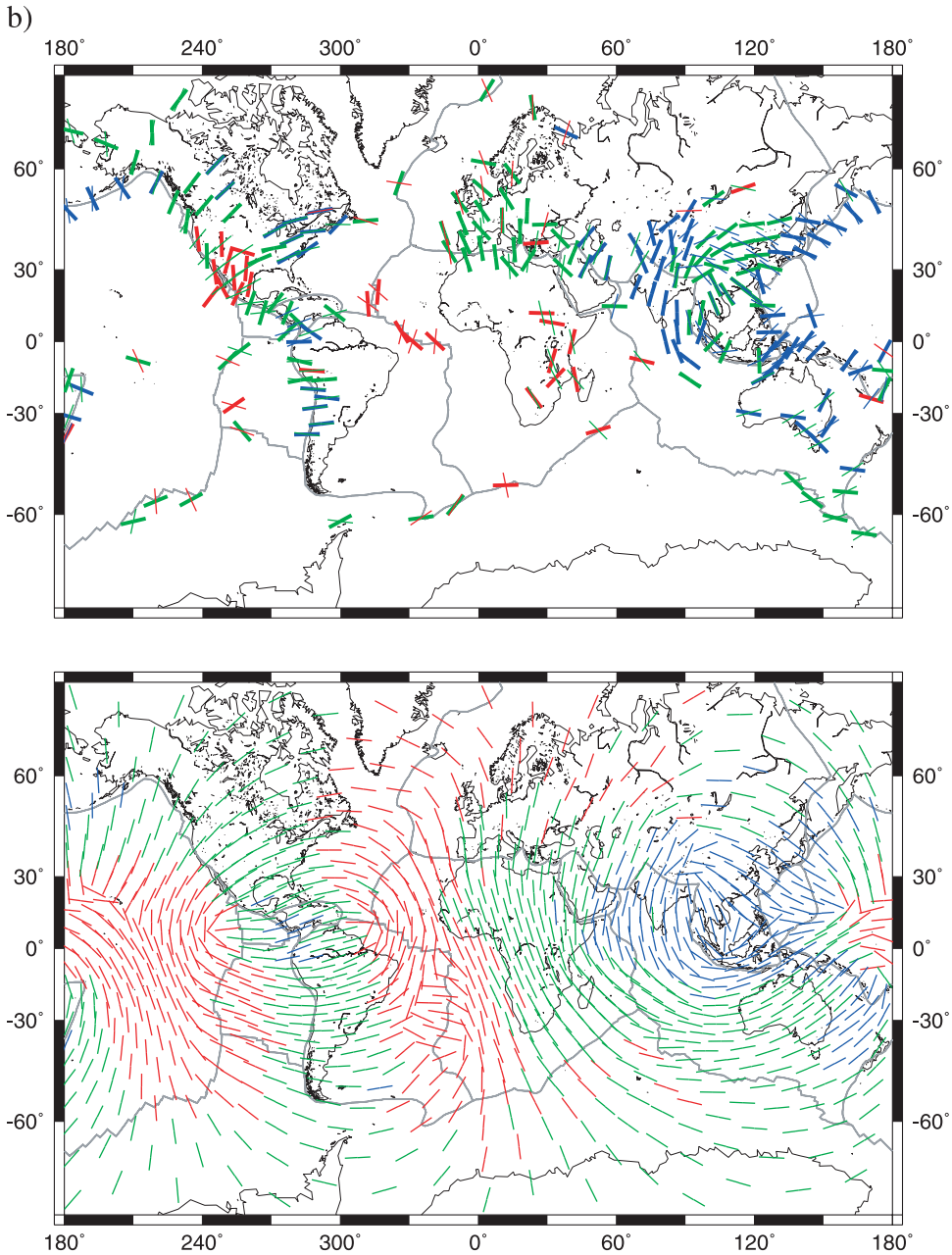

Figure 19. (continued)

is that more of the globe is now characterized by a normal or thrust regime than in model SLB + TD0.

[57] Model TMG + TD0 (Figure 19c) is substantially worse than LVC + TD0, SLB + TD0, or the other mantle models in variance reduction in azimuth (32%) although is it comparable to LVC + TD0 in variance reduction of the regime data (60%). This pattern is born out by regional comparisons which show that TMG + TD0 to be inferior in azimuth and somewhat superior in regime (Table 3). Our results for TMG are similar to those of *Steinberger et al.* [2001].The influence of Farallon subduction is much stronger in TMG than in either SLB or LVC, producing large regions of thrust regime in the Americas, and leading to better agreement with observations in northwestern Canada, and the mid-North American plate. Some normal regime is produced in the western United States, although the extensional direction (N-S) is opposite to that observed in the Basin and Range. Active upwelling beneath Africa produces N-S extension in eastern and southern Africa, in agreement with observations. The pattern of stresses in southern Asia in TMG is very different from that in SLB or LVC so that azimuths are dominantly E-W in this region, in poor agreement with observations. A prominent feature of the models that combine mantle contributions from subduction history with TD0 is a ring of compressive stress in Southeast Asia with $\tau_{H\max}$ dominantly tangent to the circle. This pattern is due to strong convergent flow centered on Taiwan from Paleotethys subduction (Figure 7). In the tomographic model of *Grand et al.* [1997] the signal of the subduction in this region is muted and the associated

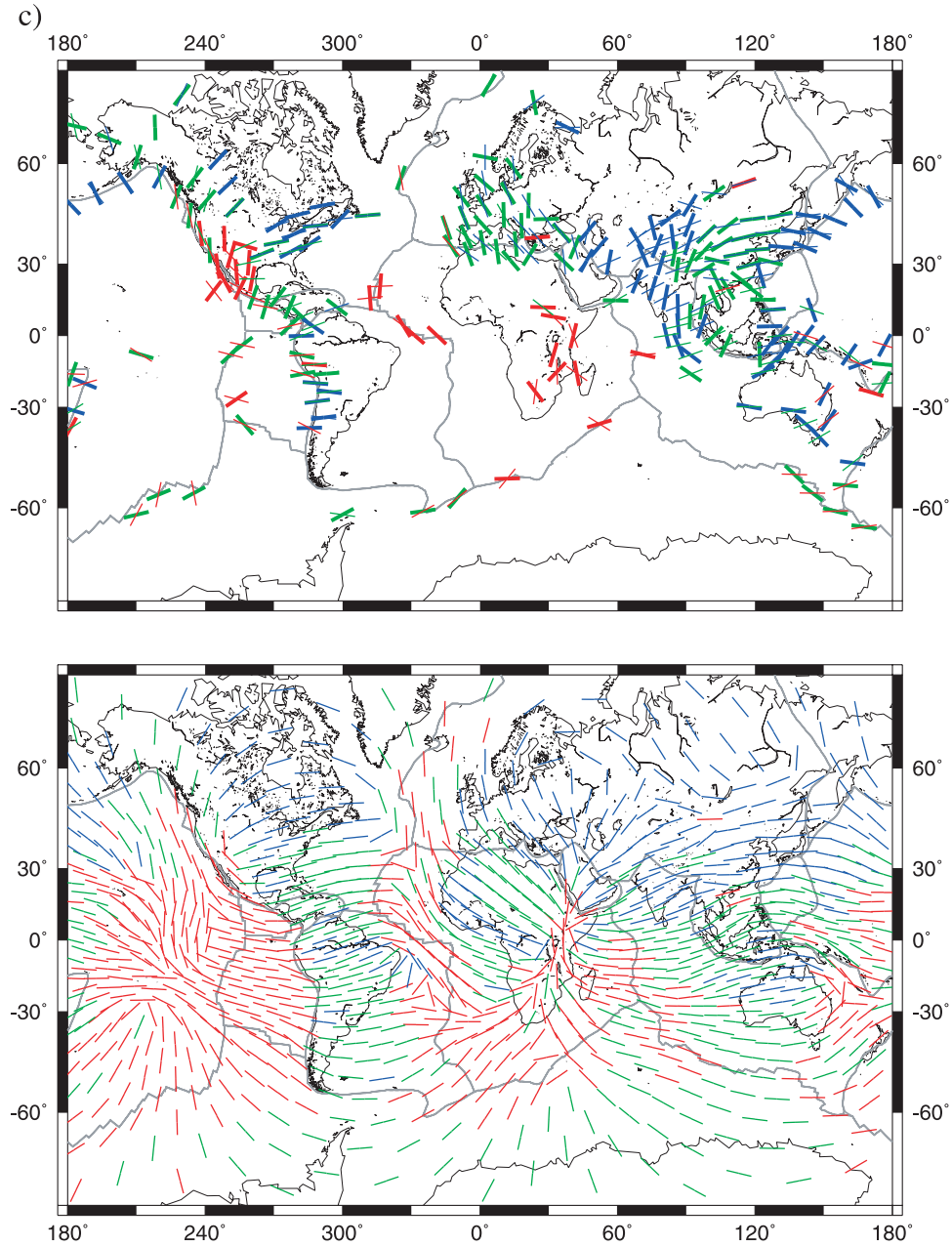

Figure 19. (continued)

ring of compressive stress is absent from model TMG + TD0. This leads to poor agreement with observations between TMG + TD0 and observations in the Indian Ocean and India. The model TMG + TD0 predicts a dominantly NW-SE compressive stress regime in Europe in better agreement with observations than other models, which produce tensional stresses in this region.

[58] The two crustal models (TD0 and TD5) are very different in their ability to reproduce observations (Figures 19d and 19e). While TD0 shows global and regional agreement similar to the mantle models, TD5 shows little agreement in azimuth or regime. Model TD0 shows a general area of ENE-WSW compression in eastern North America; the $\tau_{H\max}$ direction rotates counterclockwise around the Gulf of Mexico and around Alaska, showing extension in western Mexico, as observed. The change in stress regime from dominantly compressive to dominantly extensional in western North America and Mexico is due to (1) higher topography, (2) the ocean-continent density contrast along the Pacific coast, and (3) the westward aging of the Pacific and the associated ridge-push, which is in part transmitted to the continent. South America is dominantly in E-W compression except for the highest parts of the Andes, which show N-S extension. There are also some observations of N-S trending compressive directions in north central South America, but these may be due to local effects of an ancient failed rift [*Zoback and Richardson*, 1996]. In western Europe, $\tau_{H\max}$ directions are dominantly NW, in India NNE and in Australia, ENE to NE, which are consistent with the observations. The

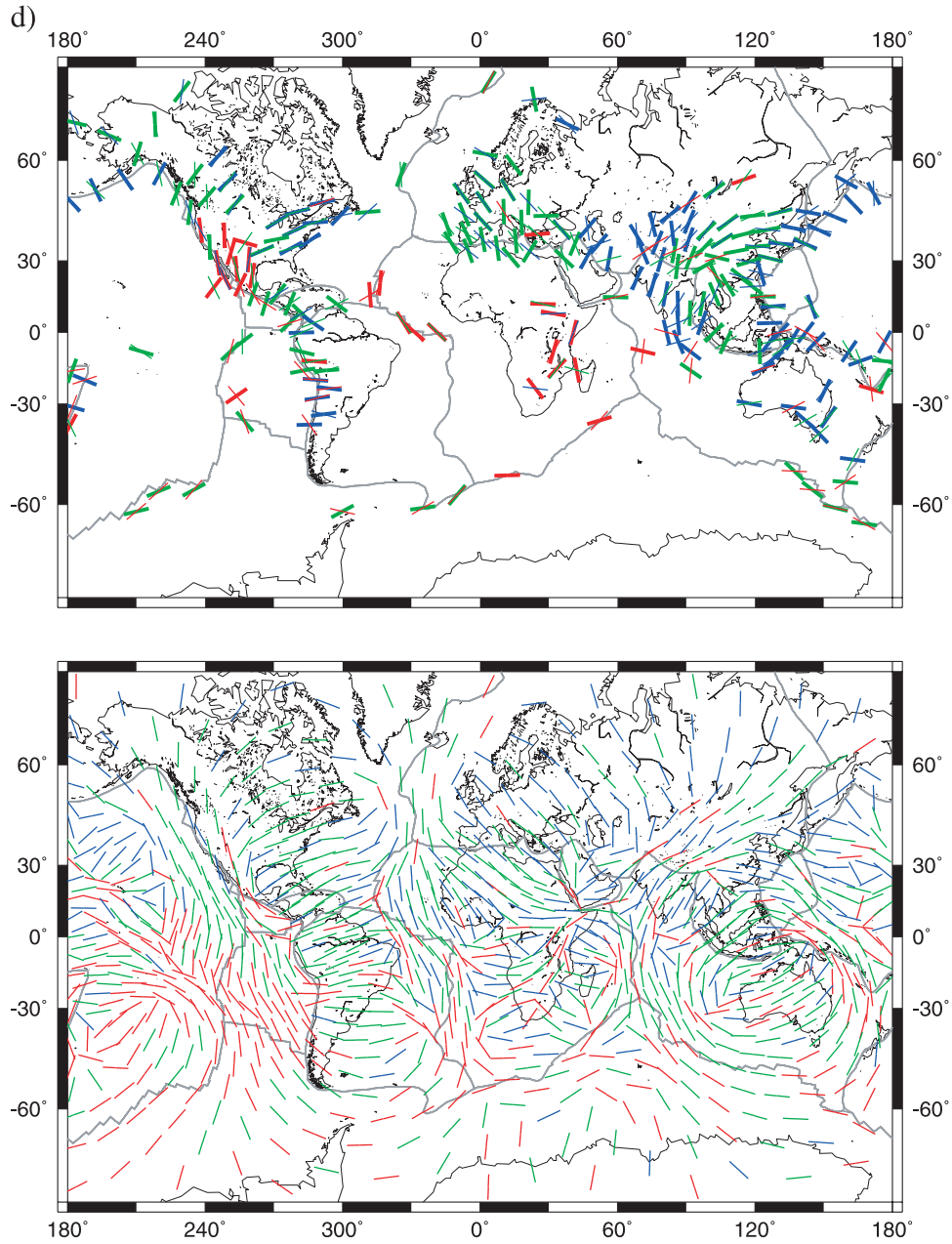

Figure 19. (continued)

model also correctly predicts NW-SE extension in the rift zone of Africa and radiation of the $\tau_{H\max}$ direction outward from the topographic high in Ethiopia. In Tibet, TD0 predicts regional NE compression with NW extension in the Himalayas. Observations show a similar pattern, although observed $\tau_{H\max}$ directions are somewhat more northward than those predicted. The NW-SE extension in the Lake Baikal region is correctly captured by TD0, as is the dominantly ENE $\tau_{H\max}$ direction in northeastern China.

[59] There are some regions of significant discrepancy between model TD0 and observations. In California, the predicted $\tau_{H\max}$ direction is almost parallel to the San Andreas fault, rather than normal to it, as observed. The ENE $\tau_{H\max}$ direction in northeastern Alaska is not predicted. The model does not predict the observed E-W extension in the southeastern Europe and Turkey, nor the N-S $\tau_{H\max}$ direction in the South China Sea or the NW-SE $\tau_{H\max}$ direction in southeastern Australia. Moment tensor analysis indicates a NW compressive direction in the east Indian Ocean, while TD0 predicts very small stresses in this region and a $\tau_{H\max}$ direction normal to that observed. Some of this latter discrepancy may be due to local topography on a scale not resolved by the model.

[60] Model TD5 does not match observations nearly as well as model TD0. Because isostatic balance is enforced in TD5, the stress regime in most continents is substantially more extensional than in model TD0. Tibet shows stresses with extensional to strike-slip sense, and no compressional stresses are observed, although compression is expected at the margins of the plateau. In western South America, the

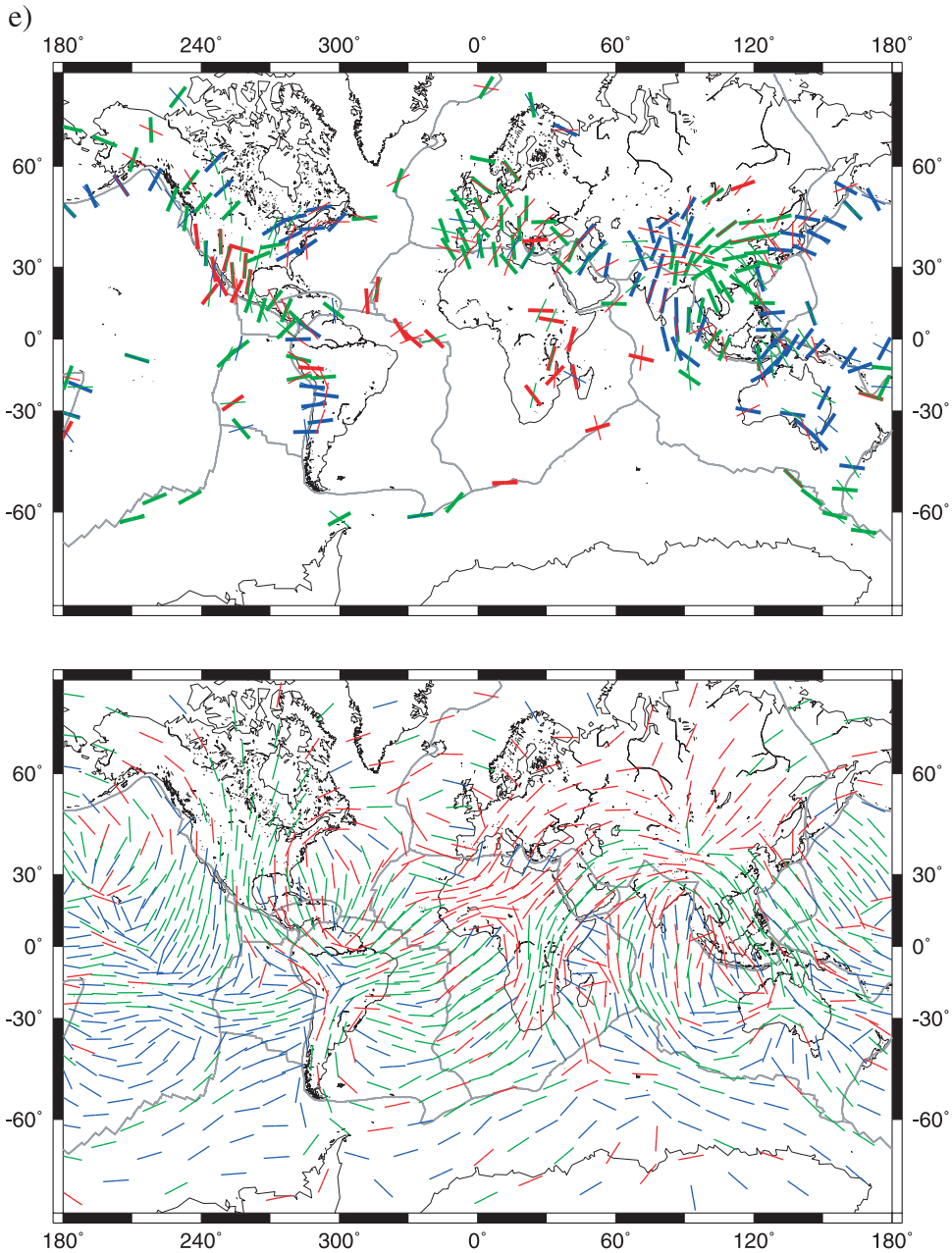

Figure 19. (continued)

sense of stress is extensional to strike slip throughout and not only in the regions of high elevation. In Africa, extensional regimes are predicted nearly for the whole continent rather than only in the rift valley. Regions near ridges are more in compression in TD5 and there is an area of compression in eastern and southeastern Asia that is much stronger than in TD0.

[61] The relative success of model TD0 (43% variance reduction in azimuth, 46% in regime) is somewhat surprising, since the continents are not in isostatic balance. This isostatic disequilibrium means that (1) the crustal structure in Crust 2.0 is incorrect, (2) there is a significant lithospheric component of compensation missing, or (3) there is some physical mechanism that keeps the crust out of balance, such as dynamic topography. Adjustment of the Crust 2.0 data for any of these would result in a change in the stress field, which would likely reduce the fit to observations. This is in fact observed with model TD5, which had the worst fit of all the models, despite being isostatically balanced. The addition of the TD0 stresses to the LVC stresses, which includes the effect of dynamic topography, improves the fit relative to LVC, and this combined model yields the best quantitative fit to the data. However, it is interesting to note that the regions where TD0 has the worst fit are the regions that the LVC model has the best fit, namely the Indo-Australian plate and Asia. In this area of concentrated and long-lived subduction and large dynamic topography, mantle tractions are clearly an important contribution to the stress field and substantially more important than crustal contributions. The lateral variation in the importance of the

mantle and lithospheric component suggest that there are strong lateral and perhaps vertical variations in rheology that affect the coupling between lithosphere and mantle or between upper and lower lithosphere.

[62] The favorable comparison of TD0 and observations must be judged conservatively, particularly when trying to separate causes from effects. For instance, in extensional zones such as the East African rift system, the tectonic process of extension always produces high topography parallel to the rift valley as well as higher average lithospheric density due to the crust being thinned and replaced with denser mantle material. In turn, this gravitational potential energy will always result in a prediction of rift normal extension, regardless of the forces actually responsible for the rift. In another case, the Tibetan Plateau combined with the change from the Indian subcontinent to the Indian Ocean is a large source of gravitational potential energy pushing the Indian plate away from Asia, yet the Indian plate is continuing to move northward.

[63] The differences between models TD0 and TD5 suggest as a possibility that in some regions the stresses observed at the surface only represent upper crustal stresses, and that sources of stress lower in the lithosphere, whether from mantle or lithospheric inhomogeneity, have little effect on stress measurements. Such a decoupling would explain why mantle tractions in the Indonesian region better match observations, but not necessarily elsewhere. Dynamic topography is large in Southeast Asia, independent of the viscosity structure of the mantle.

[64] We also need to exert caution in the interpretation of quantitative comparisons. Such comparisons can be misleading, as the coverage of the Earth's surface from the WSM map is minimal (21%). Essentially any quantitative or qualitative comparison with the WSM is primarily an assessment of how well we can reproduce the stress state of the continents. Also, continents are the most challenging part of the system to model, given their large degree of inhomogeneity in thickness, composition and material properties. Except for a few regions, the large gaps in the stress data make it hard to discern long wavelength patterns, such as those generated by mantle tractions, and leave open the possibility that isolated stress measurements may be strongly influenced by local density or topography. The relative paucity of oceanic data is particularly troublesome, as this represents the majority of the Earth's surface and the fastest moving plates have little, if any, continental material. This is especially unfortunate since the homogeneity of oceanic crust and lithosphere would result in less local effects on the stress directions and would help in resolving the different relative contributions to the stress field. There is also a concentration of data near plate boundaries, which have more complex mechanics, such as flexural bending, and where the majority of measurements are from earthquake data, which may reflect kinematics more than the forces on the plate. For example, the majority of earthquakes at or near ridges in the WSM indicate normal faulting perpendicular to the ridges. This does not fit the extensional tectonics of ridges, where the faulting is parallel to the ridges, and would not be predicted by oceanic lithosphere cooling. They may be simply a result of earthquakes along fracture zones due to differences in plate ages. In the Indian Ocean, the earthquakes may actually be a reflection of the presence of a diffuse plate boundary zone that accommodates the deformation between the Indian and Capricorn plates [*Tinnon et al.*, 1995; *Royer and Gordon*, 1997; *Kreemer et al.*, 2003]. Even in some continental areas, such as western Europe, most measurements give a consistent $\tau_{H\max}$ direction, but all three styles of faulting are represented in the same area. Nonetheless earthquake focal mechanisms tend to reflect the large-scale kinematics and thus presumably the dynamics of the region.

[65] The model we have presented is simplified and does not capture all the physics of the problem. For example, we have not included all edge tractions acting at plate boundaries. Perhaps more importantly the mantle heterogeneity model [*Ricard et al.*, 1993; *Lithgow-Bertelloni and Richards*, 1998] does not treat slabs as coherent units but rather as detached Stoke blobs sinking into the mantle, and does not include positive buoyancy due to large-scale upwellings. The rheology of the slab may have substantial influence on the state of stress in the plate and at the plate boundary via the stress guide effect. Indeed we have indication this is the case from double seismic zones attributed to the bending and unbending of plates [*Conrad and Hager*, 1999], the larger speeds of subducting plates compared to nonsubducting plates [*Conrad and Lithgow-Bertelloni*, 2002] and the correlation between the amount of slab pull and the state of stress in the back arc [*Conrad et al.*, 2003]. The approximation in our models that would be most difficult to surpass satisfactorily will be that of lithospheric rheology. Variations of lithospheric strength both laterally and vertically may have a significant effect on the stress directions. However, how to adequately constrain these changes in rheology of plates and particularly of continents? Lateral variations in rheology away from plate boundaries, such as are manifested in the presence of deep continental roots, may affect the shear tractions under continents, as well as the crustal contributions to stress in these regions. Finally, lack of constraints on the structure of the lower crust and lithosphere of the continents complicate the accurate determination of the effects of density and topography for continental regions. The constant thickness of the lithosphere in our models would only affect the magnitudes and not the directions of predicted stresses for linear rheologies.

[66] In the future, models will include variations in actual lithospheric thicknesses and lateral and vertical variations in rheological properties. The difficulty is not in the implementation but in the determination of the appropriate parameters. We will look at the effect of major edge tractions by including the effects of slab rheology in our models, both as a direct force acting at the edge of subducting plates, and through its effect on mantle tractions. Fault elements or resistive edge tractions at collisional and transform boundary may be implemented by minor modifications of the basic model. Focusing on specific regions within the global picture might help us better unravel the mantle contributions from the local effects of topography and density. Finally, including vertical variations in the strength of the lithosphere might give us the means to ascertain whether certain stress measurements represent the state of stress of the plate or only of the upper crust. Such calculations would allow us to further examine the degree of coupling between the upper and lower parts of the

lithosphere, as well as their degree of coupling to the mantle.

7. Conclusions

[67] The results of our modeling on the most important sources of stress in the lithosphere at long wavelengths leaves us with a complex picture of the origin of the lithospheric stress field. Given the degree of rheological complexity of plates and continental regions in particular, this result is perhaps not entirely surprising.

[68] We find that a combined model that includes both mantle and lithospheric sources of stress yields the best match to the observed stress field (62% variance reduction) although there are many regions where agreement between observed and predicted stresses is poor. The stress field produced by mantle tractions alone shows a greater degree of long-wavelength structure than is apparent in the stress observations, but agrees very well with observations in some areas where radial mantle tractions are particularly strong such as in southeast Asia and the western Pacific. The stress field produced by lithospheric heterogeneity alone depends strongly on the assumed crustal model: whereas the isostatically compensated model yields very poor agreement with observations, the model based on Crust 2.0 matches the observations almost as well as mantle tractions alone, and matches very well in certain areas where the influence of high topography is very important (e.g., Andes, East Africa).

[69] It seems surprising at first that a model of mantle density heterogeneity and flow that accurately reproduces global geophysical observables, such as the plate velocity and gravity field, and hence accounts for most plate driving forces [*Lithgow-Bertelloni and Richards*, 1998], should not also reproduce surface observations of the stress field. Our results show, however, that the stress field computed from mantle flow alone shows a much greater preponderance of very long wavelength spatial variations than the WSM, regardless of assumed viscosity structure or density heterogeneity field. Moreover, lateral variations in lithospheric rheology, such as those expected at plate boundaries, do not seem to alter the stress patterns significantly.

[70] The more rapid spatial variability of the observed stress field suggests an important role for sources of stress due to lithospheric heterogeneity. However, an isostatic model of the crust, based on observations (TD5) provides the worst fit to the observed stress field. A variance reduction of ~40% (Tables 1 and 2) is achieved by using only lithospheric contributions derived from the crustal and density structure of Crust 2.0 without enforcing isostasy (TD0). Although we do not expect all continents (or oceans) to be completely balanced isostatically, it is unlikely that TD0 represents the full lithospheric density structure, and the differences between the two crustal models may largely be due to remaining uncertainties in crustal structure and rheology. We think it more likely that the poor fit between the isostatically compensated crustal model and observations means that not all topography is isostatically compensated and points toward detectable dynamic topography on continents and oceans (absent in TD5), and hence that mantle tractions associated with dynamic uplift and subsidence make important contributions to the stress field.

[71] Our modeling may suggest that observations of stress from the shallow crust may not be representative of the state of stress of the entire lithosphere. Shallow stresses may be at least partially decoupled from broader-scale plate driving forces by lateral and vertical variations in lithospheric rheology. Particularly, WSM observations may only represent the upper part of the lithosphere and deeper sources of stress may be decoupled from the surface and not influence the observed azimuth and regime. This decoupling implies strong depth dependence to the rheology of the lithosphere, in the form of a weaker lithospheric layer, possibly the ductile region of the lower crust. The presence of this layer implies a depth dependence to stress orientations as seen by *Lynch and Richards* [2001]. Decoupling from deeper sources cannot be ubiquitous, however, as the stress observations cannot be matched without considering mantle tractions in the Indo-Australian and western Pacific regions.

[72] A region-by-region comparison of our models suggests that the relative importance of mantle and lithospheric contributions to the stress field may vary laterally. While neither mantle nor lithospheric sources alone provide a good global match to the WSM observations, each provide an excellent match to observations in certain regions. So for example, the strong radial mantle tractions in southeast Asia and the western Pacific account well for the observed stress regime there. Similarly, lithospheric heterogeneity alone accounts well for the stress regime in East Africa and the Andes. The relative importance of mantle and lithospheric contributions are influenced by rheology: for example, adding a low-viscosity channel mutes the mantle contributions while leaving the lithospheric contributions unaffected. The regional pattern of agreement that we find suggests that lateral variations in mantle as well as lithospheric rheology may be important for understanding the global stress field. Lateral variations in mantle viscosity would lead to variable amounts of decoupling between lithosphere and mantle, allowing the mantle signature to dominate in some areas, and the crustal signature to dominate in others.

[73] We speculate that the strong geographical variations we observe in the contribution of lithospheric and mantle sources of stress to the stress field may lead us to a global quantification of lateral and vertical variations in rheology in both the lithosphere and the shallow mantle.

[74] One may conclude that given the scarcity of stress directions over most of the plates and the uncertainties in the data that it may not be possible to unravel the different contributions to the stress field or to distinguish between models of plate driving forces with the available stress data any better than using other global geophysical observables. However, this last pessimistic conclusion is only meant as a cautionary note, to avoid overinterpretation of the present results. In fact, for forward predictive models such as those presented here, with no parameters adjusted to fit the data, variance reductions on the order of 50% and higher are extremely good. As our models become more sophisticated and our ability to incorporate constraints rise so will our optimism.

[75] **Acknowledgments.** We thank L. Ruff, C. P. Conrad, and L. Stixrude for fruitful discussions and comments. We thank the Associate Editor and two anonymous reviewers for insightful reviews that enriched and improved the manuscript. We thank Peter van Keken for providing the mesh-generating algorithm. Maps were prepared using GMT version 3.4.2

by P. Wessel and W. F. Smith. This work was supported by NSF grant EAR-9980551 awarded to Lithgow-Bertelloni.

References

Artyushkov, E. V. (1973), Stresses in the lithosphere caused by crustal thickness inhomogeneities, *J. Geophys. Res.*, *78*, 7675–7708.

Bai, W., C. Vigny, Y. Ricard, and C. Froidevaux (1992), On the origin of deviatoric stresses in the lithosphere, *J. Geophys. Res.*, *97*, 11,729–11,737.

Bird, P. (1988), Formation of the Rocky Mountains, western United States: A continuum computer model, *Science*, *239*, 1501–1507.

Bird, P. (1998), Testing hypotheses on plate-driving mechanisms with global lithosphere models including topography, thermal structure and faults, *J. Geophys. Res.*, *103*, 10,115–10,129.

Bird, P., and Y. Li (1996), Interpolation of principal stress directions by nonparametric statistics: Global maps with confidence limits, *J. Geophys. Res.*, *101*, 5435–5443.

Cazenave, A., A. Souriau, and K. Dominh (1989), Global coupling of Earth surface topography with hotspots, geoid and mantle heterogeneities, *Nature*, *340*, 54–57.

Coblentz, D. D., and R. M. Richardson (1995), Statistical trends in the intraplate stress field, *J. Geophys. Res.*, *100*, 20,245–20,255.

Coblentz, D. D., and R. M. Richardson (1996), Analysis of the South American intraplate stress field, *J. Geophys. Res.*, *101*, 8643–8657.

Coblentz, D. D., and M. Sandiford (1994), Tectonic stresses in the African plate: Constraints on the ambient lithospheric stress state, *Geology*, *22*, 831–834.

Coblentz, D. D., S. Zhou, R. R. Hillis, R. M. Richardson, and M. Sandiford (1998), Topography, boundary forces, and the Indo-Australian intraplate stress field, *J. Geophys. Res.*, *103*, 919–931.

Colin, P., and L. Fleitout (1990), Topography of the ocean floor: Thermal evolution of the lithosphere and interaction of mantle heterogeneities with the lithosphere, *Geophys. Res. Lett.*, *17*, 1961–1964.

Conrad, C. P., and B. H. Hager (1999), Effects of plate bending and fault strength at subduction zones on plate dynamics, *J. Geophys. Res.*, *104*, 17,551–17,572.

Conrad, C. P., and C. Lithgow-Bertelloni (2002), How slabs drive plate tectonics, *Science*, *298*, 207–209.

Conrad, C. P., S. Bilek, and C. Lithgow-Bertelloni (2003), Great earthquakes and slab pull: Interaction between seismic coupling and plate-slab coupling, *Earth Planet. Sci. Lett.*, in press.

DeMets, C., and T. H. Dixon (1999), New kinematic models for Pacific-North America motion from 3 Ma to present: 1. Evidence for steady motion and biases in the NUVEL-1A model, *Geophys. Res. Lett.*, *26*, 1921–1924.

DeMets, C., R. G. Gordon, D. F. Argus, and S. Stein (1990), Current plate motions, *Geophys. J. Int.*, *101*, 435–478.

Fischer, K. M. (2002), Waning buoyancy in the crustal roots of old mountains, *Nature*, *417*, 933–936.

Fleitout, L. (1991), The sources of lithospheric tectonic stresses, *Philos. Trans. R. Soc. London, Ser. A*, *337*, 73–81.

Fleitout, L., and C. Froidevaux (1982), Tectonics and topography for a lithosphere containing density heterogeneities, *Tectonics*, *1*, 21–56.

Fleitout, L., and C. Froidevaux (1983), Tectonic stresses in the lithosphere, *Tectonics*, *2*, 315–324.

Flesch, L. M., W. E. Holt, A. J. Haines, and B. Shen-Tu (2000), Dynamics of the Pacific-North American plate boundary in the western United States, *Science*, *287*, 834–836.

Flesch, L. M., A. J. Haines, and W. E. Holt (2001), Dynamic of the India-Eurasia collision zone, *J. Geophys. Res.*, *106*, 16,435–16,460.

Forsyth, D. W., and S. Uyeda (1975), On the relative importance of driving forces of plate motion, *Geophys. J. R. Astron. Soc.*, *43*, 163–200.

Forte, A. M., A. M. Dziewonski, and R. L. Woodward (1993), Aspherical structure of the mantle, tectonic plate motions, non-hydrostatic geoid, and topography of the core-mantle boundary, in *Dynamics of the Earth's Deep Interior and Earth Rotation*, *Geophys. Monogr. Ser.*, vol. 72, edited by J. L. LeMouël, D. E. Smylie, and T. Herring, pp. 135–166, AGU, Washington, D. C.

Fowler, C. M. R. (1990), *The Solid Earth: An Introduction to Global Geophysics*, Cambridge Univ. Press, New York.

Gordon, R. G. (1995), Plate motions, crustal and lithospheric mobility, and paleomagnetism: Prospective viewpoint, *J. Geophys. Res.*, *100*, 24,367–24,392.

Govers, R., and P. T. Meijer (2001), On the dynamics of the Juan de Fuca plate, *Earth Planet. Sci. Lett.*, *189*, 115–131.

Grand, S., R. D. van der Hilst, and S. Widiyantoro (1997), Global seismic tomography: A snapshot of convection in the Earth, *GSA Today*, *7*, 1–7.

Hager, B. H., and R. J. O'Connell (1979), Kinematic models of large-scale flow in the earth's mantle, *J. Geophys. Res.*, *84*, 1031–1048.

Hager, B. H., and R. J. O'Connell (1981), A simple global model of plate dynamics and mantle convection, *J. Geophys. Res.*, *86*, 4843–4867.

Hibbit, K., and Sorenson (2002), ABAQUS, versions 6.2, Pawtucket, R.I.

Jeffreys, H. (1959), *The Earth*, 4th ed., Cambridge Univ. Press, London.

Jones, C. H., J. R. Unruh, and L. J. Sonder (1996), The role of gravitational potential energy in active deformation in the southwestern United States, *Nature*, *381*, 37–41.

Kreemer, C., W. E. Holt, and A. J. Haines (2003), An integrated global model of present-day plate motions and plate boundary deformation, *Geophys. J. Int.*, *154*, 1–27.

Le Stunff, Y., and Y. Ricard (1995), Topography and geoid due to lithospheric mass anomalies, *Geophys. J. Int.*, *122*, 982–990.

Lithgow-Bertelloni, C., and M. A. Richards (1998), The dynamics of Cenozoic and Mesozoic plate motions, *Rev. Geophys.*, *36*, 27–78.

Lithgow-Bertelloni, C., and P. G. Silver (1998), Dynamic topography, plate driving forces, and the African superswell, *Nature*, *395*, 269–273.

Liu, L., and M. D. Zoback (1992), The effect of topography on the state of stress in the crust: Application to the site of the Cajon pass scientific drilling project, *J. Geophys. Res.*, *97*, 5095–5108.

Liu, Y., S. Crampin, and R. E. Abercrombie (1997), Shear-wave anisotropy and the stress field from borehole recordings at 2.5 km depth at Cajon Pass, *Geophys. J. Int.*, *129*, 439–449.

Love, A. E. H. (1944), *A Treatise on the Mathematical Theory of Elasticity*, 4th ed., Dover, Mineola, N. Y.

Lynch, J. C., and M. A. Richards (2001), Finite element models of stress orientations in well-developed strike-slip fault zones: Implications for the distribution of lower crustal strain, *J. Geophys. Res.*, *106*, 26,707–26,729.

Mardia, K. V. (1972), *Statistics of Directional Data*, Academic, San Diego, Calif.

Meijer, P. T., and M. J. R. Wortel (1992), The dynamics of motion of the South American plate, *J. Geophys. Res.*, *97*, 1915–1932.

Meijer, P. T., R. Govers, and M. J. R. Wortel (1997), Forces controlling the present-day state of stress of the Andes, *Earth Planet. Sci. Lett.*, *148*, 157–170.

Molnar, P., and H. Lyon-Caen (1988), Some simple physical aspects of the support, structure, and evolution of mountain belts, *Spec. Pap. Geol. Soc. Am.*, *218*, 179–207.

Müller, R. D., W. R. Roest, J. Y. Royer, L. M. Gahagan, and J. G. Slater (1994), A digital map of the ocean floor, *SIO Ref. Ser. 93–30*, Scripps Inst. of Oceanogr., La Jolla, Calif.

Newman, A., S. Stein, J. Weber, J. Engeln, A. Mao, and T. Dixon (1999), Slow deformation and lower seismic hazard at the New Madrid seismic zone, *Science*, *284*, 619–621.

Ricard, Y., and C. Vigny (1989), Mantle dynamics with induced plate tectonics, *J. Geophys. Res.*, *94*, 17,543–17,560.

Ricard, Y., C. Vigny, and C. Froidevaux (1989), Mantle heterogeneities, geoid, and plate motion: A Monte Carlo inversion, *J. Geophys. Res.*, *94*, 13,739–13,754.

Ricard, Y., M. A. Richards, C. Lithgow-Bertelloni, and Y. LeStunff (1993), A geodynamical model of mantle density heterogeneity, *J. Geophys. Res.*, *98*, 21,895–21,909.

Richards, M. A., Y. Ricard, C. Lithgow-Bertelloni, G. Spada, and R. Sabadini (1997), An explanation for Earth's long-term rotational stability, *Science*, *275*, 372–375.

Richardson, R. M. (1992), Ridge forces, absolute plate motions, and the intraplate stress field, *J. Geophys. Res.*, *97*, 1739–1748.

Richardson, R. M., and B. L. Cox (1984), Evolution of oceanic lithosphere: A driving force study of the Nazca plate, *J. Geophys. Res.*, *89*, 10,043–10,052.

Richardson, R. M., and L. M. Reding (1991), North American plate dynamics, *J. Geophys. Res.*, *96*, 12,201–12,223.

Richardson, R. M., S. C. Solomon, and N. H. Sleep (1976), Intraplate stress as an indicator of plate tectonic driving forces, *J. Geophys. Res.*, *81*, 1847–1856.

Richardson, R. M., S. C. Solomon, and N. H. Sleep (1979), Tectonic stress in the plates, *Rev. Geophys.*, *17*, 981–1019.

Royer, J.-Y., and R. G. Gordon (1997), The motion and boundary between the Capricorn and Australian plates, *Science*, *277*, 1260–1274.

Ruff, L. J. (2002), State of stress within the Earth, in *International Handbook of Earthquake and Engineering Seismology, Int. Geophys. Ser.*, vol. 81A, edited by W. H. K. Lee et al., p. 33, Academic, San Diego, Calif.

Scholz, C. H., and F. J. Saucier (1993), What do the Cajon Pass stress measurements say about stress on the San Andreas fault?, *J. Geophys. Res.*, *98*, 17,867–17,869.

Simpson, R. W. (1997), Quantifying Anderson's fault types, *J. Geophys. Res.*, *102*, 17,909–17,919.

Solomon, S. C., N. H. Sleep, and R. M. Richardson (1975), On the forces driving plate tectonics: Inferences from absolute plate velocities and intraplate stress, *Geophys. J. R. Astron. Soc.*, *42*, 769–801.

Steinberger, B., H. Schmeling, and G. Marquart (2001), Large-scale lithospheric stress field and topography induced by global mantle circulation, *Earth Planet. Sci. Lett.*, *186*, 75–91.

Tinnon, M. J., W. E. Holt, and A. J. Haines (1995), Velocity gradients in the northern Indian Ocean inferred from earthquake moment tensors and relative plate velocities, *J. Geophys. Res.*, *100*, 24,315–24,329.

Townend, J., and M. D. Zoback (2000), How faulting keeps the crust strong, *Geology*, *28*, 399–402.

Turcotte, D. L., and G. Schubert (1982), *Geodynamics: Applications of Continuum Physics to Geological Problems*, 1st ed., Cambridge Univ. Press, New York.

Wallace, M. H., and H. J. Melosh (1994), Buckling of a pervasively faulted lithosphere, *Pure Appl. Geophys.*, *142*, 240–261.

Weber, J., S. Stein, and J. Engeln (1998), Estimation of intraplate strain accumulation in the New Madrid seismic zone from repeat GPS surveys, *Tectonics*, *17*, 250–266.

Wortel, M. J. R., M. J. N. Remkes, R. Govers, S. A. P. L. Cloetingh, and P. T. Meijer (1991), Dynamics of the lithosphere and the intraplate stress-field, *Philos. Trans. R. Soc. London, Ser. A*, *337*, 111–126.

Yoshida, M., S. Honda, M. Kido, and Y. Iwase (2001), Numerical simulation for the prediction of plate motions: Effects of lateral viscosity variations in the lithosphere, *Earth Planets Space*, *53*, 709–721.

Zhong, S., and M. T. Zuber (2000), Long-wavelength topographic relaxation for self-gravitating planets and implications for the time-dependent compensation of surface topography, *J. Geophys. Res.*, *105*, 4153–4164.

Zhong, S., M. T. Zuber, L. Moresi, and M. Gurnis (2000), Role of temperature-dependent viscosity and surface plates in spherical shell models of mantle convection, *J. Geophys. Res.*, *105*, 1063–1082.

Zoback, M. D., and J. H. Healy (1992), In situ stress measurements to 3.5 km depth in the Cajón Pass scientific-research borehole: Implications for the mechanics of crustal faulting, *J. Geophys. Res.*, *97*, 5039–5057.

Zoback, M. L. (1992), First- and second-order patterns of stress in the lithosphere: The world stress map project, *J. Geophys. Res.*, *97*, 11,703–11,728.

Zoback, M. L., and R. M. Richardson (1996), Stress perturbation associated with the Amazonas and other ancient continental rifts, *J. Geophys. Res.*, *101*, 5459–5475.

Zoback, M. L., et al. (1989), Global patterns of tectonic stress, *Nature*, *341*, 291–298.

J. H. Guynn, Department of Geological Sciences, University of Arizona, Gould-Simpson Building, Tucson, AZ 85721, USA. (jguynn@geo.arizona.edu)

C. Lithgow-Bertelloni, Department of Geological Sciences, University of Michigan, 2534 C C Little Building, 425 E. University Avenue, Ann Arbor, MI 48109-1063, USA. (crbl@umich.edu)